

Zeitschrift: IABSE reports = Rapports AIPC = IVBH Berichte
Band: 76 (1997)

Rubrik: Theme F: Fatigue assessment

Nutzungsbedingungen

Die ETH-Bibliothek ist die Anbieterin der digitalisierten Zeitschriften auf E-Periodica. Sie besitzt keine Urheberrechte an den Zeitschriften und ist nicht verantwortlich für deren Inhalte. Die Rechte liegen in der Regel bei den Herausgebern beziehungsweise den externen Rechteinhabern. Das Veröffentlichen von Bildern in Print- und Online-Publikationen sowie auf Social Media-Kanälen oder Webseiten ist nur mit vorheriger Genehmigung der Rechteinhaber erlaubt. [Mehr erfahren](#)

Conditions d'utilisation

L'ETH Library est le fournisseur des revues numérisées. Elle ne détient aucun droit d'auteur sur les revues et n'est pas responsable de leur contenu. En règle générale, les droits sont détenus par les éditeurs ou les détenteurs de droits externes. La reproduction d'images dans des publications imprimées ou en ligne ainsi que sur des canaux de médias sociaux ou des sites web n'est autorisée qu'avec l'accord préalable des détenteurs des droits. [En savoir plus](#)

Terms of use

The ETH Library is the provider of the digitised journals. It does not own any copyrights to the journals and is not responsible for their content. The rights usually lie with the publishers or the external rights holders. Publishing images in print and online publications, as well as on social media channels or websites, is only permitted with the prior consent of the rights holders. [Find out more](#)

Download PDF: 07.08.2025

ETH-Bibliothek Zürich, E-Periodica, <https://www.e-periodica.ch>



Theme F

Fatigue Assessment

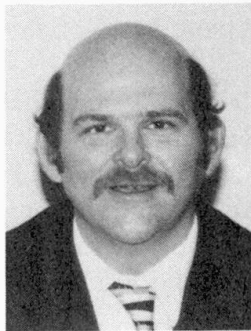
Leere Seite
Blank page
Page vide

Fatigue Cracking of Orthotropic Steel Decks

Robert J. DEXTER

Senior Research Eng.
Lehigh University
Bethlehem, PA, USA

Robert J. Dexter, born 1956, got his Ph.D. in Civil Engineering at the University of Texas at Austin. He has over 16 years experience in research on welding, fatigue, and fracture.



John. W. FISHER

Professor
Lehigh University
Bethlehem, PA, USA

John W. Fisher, born 1931, got his Ph.D. in Civil Engineering at Lehigh University and is currently director of the ATLSS Center. He is a member of the National Academy of Engineering.



Summary

A review is presented of the service fatigue-cracking problems with orthotropic steel decks in the last fifteen years; as well as available sources of fatigue test data and U.S. design recommendations. The causes of these cracking problems and the repair and retrofit procedures that were used to correct the problems are discussed. Many distortion-induced cracks can be retrofit at relatively low cost by hole drilling. Recommendations are made for fatigue-resistant weld and cutout details for future designs. A recently conducted full-scale test of a cantilevered orthotropic deck is discussed, along with recommendations for future research.

1. Introduction

The initial cost of an orthotropic steel deck is at least twice the initial cost of a 228 mm thick concrete deck. However, orthotropic steel decks are lighter and, provided they are designed to resist fatigue cracking, more durable than concrete decks. Orthotropic steel decks are also attractive for deck replacement because they can lower dead load on deteriorated superstructures and can be replaced in modules during temporary lane closures.

Structural elements in the bridge deck have very little dead load. If there are a large number of live load cycles, the fatigue limit state will generally govern the design. Bridge deck elements are loaded not just by every truck, but by every axle. Within a few years, the number of cycles of bridge deck elements can become very large, in most cases larger than the number of cycles associated with the constant-amplitude fatigue limit (CAFL) for the welded details.

Fatigue cracks have been observed in various details of orthotropic steel decks in the last fifteen years. This problem has been most severe in England, Germany, Austria, France, Japan, and Australia, particularly because thin deck plates (8 to 12 mm) were used. For the most part, the fatigue-cracking problems reflect: 1) the limited fatigue-test data on orthotropic



deck systems; and, 2) the over-optimistic definition of the fatigue strength that was attributed to these details in the 1960's and 1970's. The CAFL for most of these details was not known as relatively few tests were carried out beyond two million cycles. Hence, most of the details are subjected to service stress ranges that exceed the CAFL. Consequently, fatigue cracks develop after some time, perhaps not until after ten or more years of service.

Experimental studies of the fatigue strength of orthotropic deck details were summarized in 1989 by the Office for Research and Experiments (ORE) of the International Union of Railways in Utrecht, Netherlands [1]. This report described fatigue critical orthotropic deck details and their the fatigue strength. A second summary report was prepared by the Commission of European Communities (ECSC) [2]. This report summarizes testing and analyses from Germany, Belgium, France, Italy, Holland, and England.

2. Fatigue Design Provisions for Long-Life Variable-Amplitude Loading

The American Association of State Highway Transportation Officials (AASHTO) LRFD Bridge Design Specifications [3] contain specific guidance on the fatigue design of orthotropic steel decks. The design fatigue resistance categories of orthotropic deck details in the AASHTO LRFD recommendations are essentially the same as the recommendations in the ORE report, although there are slight differences in the fatigue strength of some details.

Typically, this fatigue design stress range is obtained from a static analysis where the wheel loads are applied in patches, and the axle load is equal to an impact factor times the design axle load. In the AASHTO LRFD specifications, an impact factor of 1.75 is recommended for deck elements. There is a great deal of uncertainty in the impact factor and the size of the wheel-load patches [4-8]. Also, due to calibration of the AASHTO LRFD specifications against previous specifications and experience, the fatigue design axle load is in fact much less than the 1:10000 exceedance level [4]. The discrepancy has been defended because it is felt that other aspects of the design process are overconservative, such as the assumptions in the structural analysis models.

The fatigue design philosophy in the U.S. for long-life (i.e. for numbers of cycles greater than the number of cycles associated with the CAFL) is to require that essentially all the stress ranges are less than the CAFL. Variable-amplitude fatigue tests on full-scale girders with welded details show that if less than 1:10,000 cycles exceed the CAFL, then essentially infinite life is obtained [9]. This approach is the basis of provisions in the AASHTO LRFD specifications, and has also been applied in developing fatigue design specifications for expansion joints [4-8], which are also loaded by every axle, and wind-loaded sign, signal, and luminaire support structures [10]. One advantage of this approach for structures with complex stress histories is that it is not necessary to accurately predict the entire future stress range histogram. The fatigue design procedure requires only the stress range with an exceedance level of 1:10,000, which is called the fatigue-limit-state stress range.

The U.S. approach for long-life variable-amplitude fatigue requires accurate definition of the CAFL. The upper part of the S-N curve is only needed for situations where the number of cycles is less than the number of cycles associated with the CAFL. These situations are referred to as being in the "finite-life" regime. For deck elements and other elements subjected to long-life loading, the emphasis in fatigue testing of details must be on defining the CAFL, which requires more expensive long-term testing at stress ranges close to service stress ranges.

The AASHTO LRFD code and the Eurocode both use an effective stress range for variable-amplitude loading (defined by Miner's rule) for use with the constant-amplitude S-N curves. However, there are large differences between the Eurocode and the AASHTO LRFD code regarding the CAFL. In the development of the U.S. codes, the CAFL has been defined as the largest stress range for which all fatigue tests are terminated with no cracking. The number of cycles associated with the CAFL is whatever number of cycles corresponds to that stress range on the S-N curve for that category or class of detail. The CAFL occurs at an increasing number of cycles for lower fatigue categories or classes. Sometimes, different details, which share a common S-N curve (or category) in the finite-life regime, have different CAFL.

The Eurocode S-N curves have a CAFL at five-million cycles regardless of the class. For variable-amplitude loading, the Eurocode S-N curves have a change in slope below the CAFL, with a cutoff at 100 million cycles.

Since both approaches are based on experimental data, it is not surprising that both result in approximately the same design for given fatigue loads [8]. Since these two approaches use different stress ranges, it is necessary to estimate a relationship between these stress ranges. Typical truck axle load spectra are such that the fatigue-limit-state stress range is typically about two times the effective stress range.

For example, using the Eurocode and considering a class 90 detail (AASHTO category C), the effective stress range should be just below the fatigue strength at 100 million cycles, which is about 40 MPa. Using the AASHTO LRFD approach, the fatigue limit-state stress range should be just below the CAFL, which is about 70 MPa for the AASHTO Category C.

3. Types of Fatigue Cracking Observed on Orthotropic Steel Decks

Generally, fatigue-cracking problems can be classified as either: 1) load-induced cracking; or, 2) distortion-induced cracking; depending on the boundary conditions of the loading which causes the stress range driving the cracking. Orthotropic steel deck cracking problems have included both types.

3.1 Load-induced cracking

The AASHTO LRFD bridge design specifications [3] cover most cases of load-induced cracking of orthotropic steel decks. Load-induced cracking is a result of the fluctuation of the nominal primary stresses, i.e. the stress range induced by the applied wheel loads using standard first-order design calculations. Load-induced cracking occurs primarily at poor details when these details are subjected to significant stress ranges exceeding the CAFL.

For example, in some early orthotropic decks, longitudinal ribs were butted up to the floor beams and fillet welded all around, as shown in Figure 1. When tension developed in the ribs, the unfused parts of the rib/diaphragm interface acted like a notch and easily cracked through the weld root. The ORE report rated the fatigue strength of this detail as the equivalent of the AASHTO Category E' with respect to the nominal longitudinal bending stress range in the rib. The cracking of this detail led to the present practice of passing the rib continuously through the diaphragm. The AASHTO LRFD code only shows the continuous-rib detail and rates the fatigue strength of this preferable detail as Category D with respect to the nominal longitudinal bending stress range in the rib.

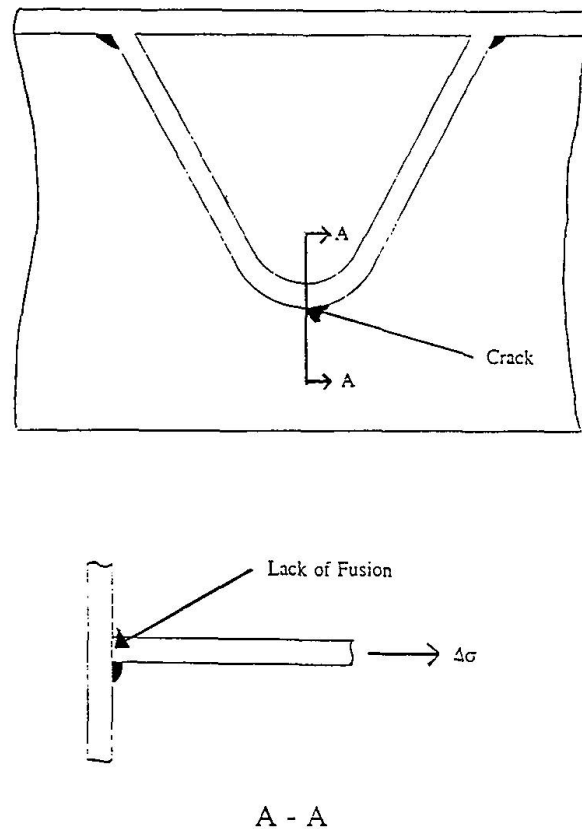


Figure 1: Fillet-welded connection of rib which is not continuous through the diaphragm

Other examples of load-induced cracking at poor details have been related to welded field splices of the longitudinal ribs. Unusually large defects in the rib splice welds have resulted in cracking. Backing bars left in place inhibit good ultrasonic testing. The AASHTO LRFD code rates the welded rib splice with a backing bar as a Category E detail. The orthotropic deck of the Rio-Niteroi Bridge in Brazil has exhibited hundreds of fatigue cracks. About 94 percent of the cracking is associated with the field-welded splices between the 15 m sections. Stress ranges were measured in these ribs in excess of the CAFL for Category E details (31 MPa).

3.2 Distortion-induced cracking

Distortion-induced cracking results from second-order stresses, typically due to out-of-plane deformations and incompatible deformations at intersecting structural elements. The stresses that cause this type of cracking are very difficult to quantify. Even detailed finite-element analyses typically cannot accurately calculate these distortion-induced stresses. Since an accurate calculation-based design method is presently not available, control of distortion-induced cracking is accomplished through the art of good detailing in addition to the standard workmanship requirements and quality control. In the AASHTO LRFD code, control of distortion-induced cracking is affected through: 1) design guidance requiring rigid load paths for possible secondary forces (such as in diaphragms); and, 2) prescriptive requirements such as minimum plate thickness.

For example, longitudinal ribs were originally welded to the deck plate using one-sided fillet welds. Figure 2 shows the transverse moments due to distortion that occur at this connection, causing prying of the unfused notch and cracking through the weld root. This problem occurred in a suspension bridge in the United Kingdom and was extensively studied by Gurney et al at The Welding Institute. Virtually all of these welds had to be gouged and rewelded. These longitudinal welds are now required to have at least 80 percent penetration. Also, the LRFD code requires the deck plate to be 16 mm or greater, and has requirements for the maximum rib thickness. The deck plate requirements assure that the distortions are minimized, and the rib thickness limits insure that the rib is flexible enough to accommodate the rotations.

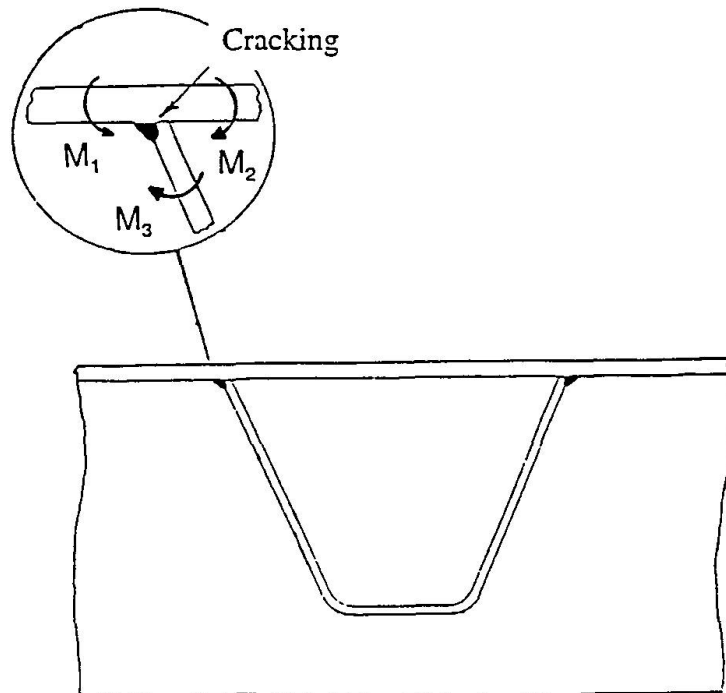


Figure 2: Distortion-induced cracking at longitudinal fillet-weld joining rib to deck plate

Distortion-induced cracking can also occur for a number of reasons in the connection of the transverse diaphragms to the continuous ribs. One such problem is due to shear deformations in the diaphragms and is particularly severe in cantilever sections due to high shear forces on tapered floor beams. Also, slow traffic lanes, with the heaviest trucks, are typically located on the ends of these cantilevers. There are some explicit design calculations for this shear problem in the AASHTO LRFD code.

Figure 3 shows some of the cracks which might occur at the diaphragm/rib connection including cracking in the cutouts and longitudinal cracking of the ribs at the intersection with the cutout. In 1990, similar longitudinal cracks were noticed in the ribs of the Westgate Bridge in Australia [11]. The ribs did not have internal diaphragms or bulkhead plates to carry the forces imparted by the floorbeam diaphragm. These cracks originated from "oil-can" deformation of the ribs by the floor-beam diaphragms. Internal bulkhead plates are now considered good practice. These bulkhead plates should be at least 12 mm thick with 8 mm fillet welds, and should be almost full depth of the rib, i.e. the bulkhead should come up as close as possible to the top of the rib and extend down as close as possible to the bottom of the rib, considering required clearance and tolerances.

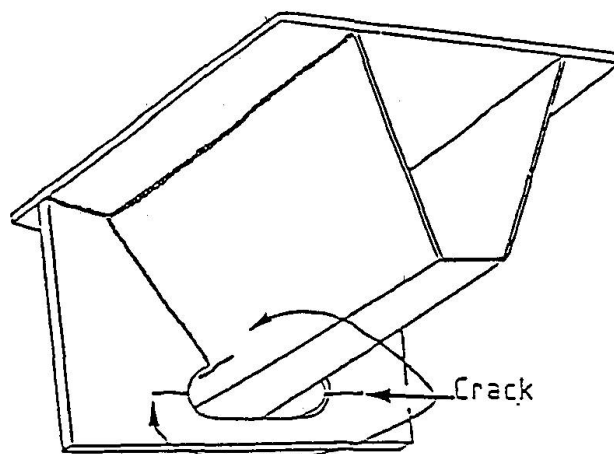


Figure 3: Diaphragm-to-rib connection showing typical crack locations at the cutout

Perhaps the most critical aspect of this diaphragm/rib connection is the termination of the fillet welds. The welds should not wrap around the diaphragm, rather, the ends of the welds should be ground. Figure 4 shows the traditional fillet weld termination detail as well as a new combination weld detail for the weld termination which was developed by Steinman Consulting Engineers for the replacement deck for the Williamsburg Bridge in New York City. The combination weld detail includes a partial length complete-penetration groove weld which is ground to a smooth transition at the intersection of the cutout. New York City Department of Transportation had a full-scale fatigue test of the proposed deck design, with both the traditional detail and the combination weld detail, conducted at the ATLSS Center at Lehigh University [12]. The unique loading scheme to simulate rolling traffic loads was developed by New York City DOT [13]. Figure 5 shows a view of the top of the deck which is on floorbeams which are cantilevered from strong wall at the ATLSS laboratory. Figure 6 shows a close-up view of a typical diaphragm with the strain gages to measure the complex distortion-induced stress ranges near the rib connection. The tests showed the improved fatigue resistance of the Option A detail.

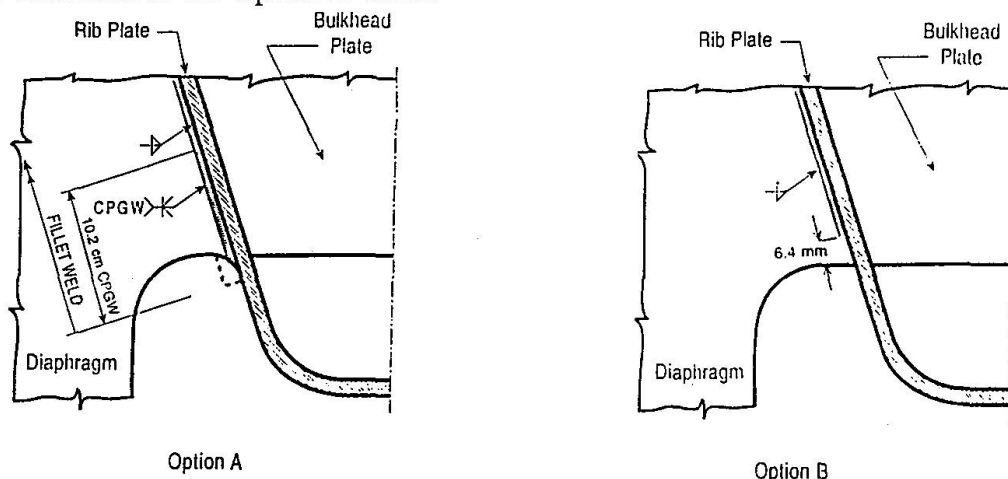


Figure 4: Alternative details for the termination of the weld in the diaphragm-to-rib connection

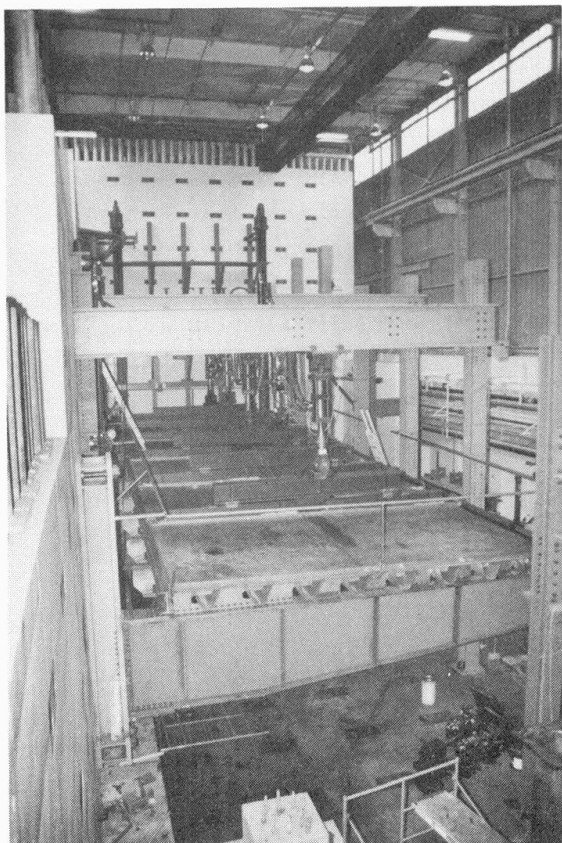


Figure 5 Full-scale fatigue test of a cantilevered section of an orthotropic deck.

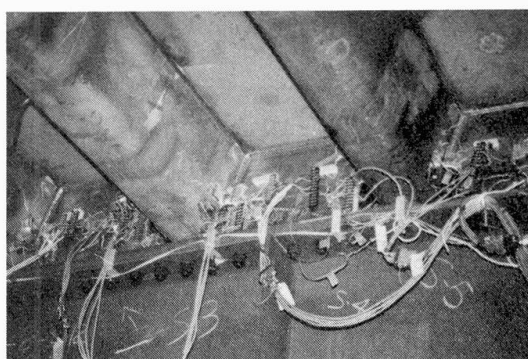


Figure 6: Typical diaphragm of the full-scale test showing strain gage locations near the rib connection.

Other recent test data, some of which are included in the ECSC report, show that fully welded details with no cutout have greater fatigue resistance than details with the cutout. Unfortunately, fit-up problems are more difficult without the cutout, therefore the decision may be made to use the cutouts despite the lower fatigue resistance.

The LRFD code has some guidance on cope holes and cutouts to reduce problems with cracking. Copes or snipes in the corner, where the diaphragm is welded to both the rib and the deck plate, are not allowed because of known fatigue problems. The distance between the bottom of the ribs and the connection to the diaphragm should be maximized.

In the United States, orthotropic decks are mostly used in redecking older bridges. A special type of distortion-induced cracking associated with redecking is caused by incompatibility between the curvatures of the rigid deck and the rather flexible floor systems. This problem usually manifests as longitudinal rotation and prying of the connection between the deck and the floorbeams (or stringers in some cases). This type of cracking has been observed on the Throg's Neck Bridge, for example. The problem was recently studied using finite-element analysis at Weidlinger and Associates.



4. Repair and Retrofit

There are a few cases where a distortion-induced crack is reasonably small, e.g. less than 75 mm, and is propagating only under the influence of secondary transverse stress ranges. These stress ranges are due to local distortion of the orthotropic deck under wheel loads. The stresses that result from the distortion decrease locally as the cracks make the section more compliant. Therefore, many of these cracks can probably be left in place after holes are drilled or cored at the tips of the crack. Coring at the tip of a crack essentially blunts the tip of the crack. Cracking will not reinitiate if the size of the hole satisfies the relationship:

$$\frac{\Delta K}{\sqrt{\rho}} \leq 10.5 \sqrt{\sigma_y}$$

where ρ is the radius of the hole, mm, and σ_y is the yield strength of the plate, MPa. ΔK is the range in the stress intensity factor ($\text{MPa}\cdot\text{m}^{1/2}$) determined from fracture mechanics analysis from the applied stress range and the crack size. The hole size required by this equation is reasonable for small stress ranges. For example, for 350 MPa yield strength and a typical crack geometry, the equation requires a hole diameter about 20 percent of the crack length for a stress range of 35 MPa. However, the dependence on stress range is strong. For the same conditions, the hole diameter must be 80 percent of the crack length for a stress range of 70 MPa. For higher stress ranges, the entire crack must be removed. Care must be taken that the hole is not a critical stress concentration in the member.

In practice, especially in these orthotropic deck cracks, the definition of the stress range and ΔK may not be possible. In this case, conservative experience-based rules of thumb must be relied upon. Most small cracks less than 50 mm long can be successfully retrofit using a 19 mm diameter hole.

For cracks which are not entirely longitudinal or for other reasons cannot be left in place, the preferred repair procedure is to gouge out the crack and fill the groove with weld metal. When a crack is to be gouged out by the air-arc process, it is a good idea to drill holes at the tips of the crack before gouging. For fillet welds which have cracked through the throat, the size of the repair weld should be increased relative to the original weld. Inadvertent gouges created by maintenance equipment may also be filled with weld metal. Small surface cracks can often be removed with a pencil grinder or disc grinder.

There are many cases where additional retrofit is required to upgrade the details, which should be applied to cracked as well as uncracked details. Cracks have occurred at bolted flanges in end plates due to prying because of the inadequate thickness of the end plates. After the cracks are drilled and weld repaired, thick doubler plates or angles should be added to these end plate connections to stiffen them.

Cracks have also occurred at lap welds for splice plates which are lapped over the sides and bottom of the trapezoidal stiffeners. These welds can be air-hammer peened. The peening may be performed only at the outer ends of the side plates and the bottom cover plate. The peening should wrap around the corner and continue for about 25 mm away from these ends. Light surface grinding following the peening improves the fatigue resistance further. Peening can repair shallow surface cracks less than a few millimeters deep. Visible cracks greater than a few millimeters deep must be repair welded.

Another example of a retrofit is the short segments of flat-bar stiffener that have been welded in some cases to the bottom of the trapezoidal stiffeners (fins). A core should be taken about 25 mm in diameter at each end of these stiffeners. The cores should include the end of the flat bar and both fillet weld ends. The core diameter may be increased within reason to remove entirely existing cracks at these stiffener ends. Cracks which extend beyond the core diameter should be repair welded prior to coring.

Another consideration is the design and maintenance of the asphalt wearing surface. Potholes and severe deterioration of the pavement can increase the dynamic wheel loads and significantly decrease the fatigue life of the orthotropic steel deck. New asphalt high-performance wearing surfaces have been developed in Europe. These types of surfaces have a tack course applied to the steel surface and a thin wearing surface on top. The experience base with this type of surface is limited, but it was used on the Normandie Bridge in France which was recently completed.

5. Conclusions

Orthotropic steel decks have had a number of fatigue cracking problems in service which can be classified as either load-induced cracking or distortion-induced cracking. Design to resist load-induced cracking problems is relatively straightforward. Most of these problems have occurred because of inadequate knowledge of the fatigue strength of the details. The correction of service load-induced cracking problems typically involves upgrading the detail, which can be very expensive.

Distortion-induced cracking problems are typically attributable to unanticipated secondary stresses. Accurately predicting the applied stress range in design for the case of distortion-induced cracking is usually not possible. Therefore, distortion-induced cracking problems are controlled through minimum plate thickness and other detailing requirements. Distortion-induced cracks can usually be retrofit at relatively low cost, e.g. by hole drilling.

6. Acknowledgements

The paper is based on case studies investigated by the authors, cases described in the literature, and cases discussed with other engineers. The authors appreciate the support of New York City Department of Transportation, New York State Department of Transportation, and Federal Highway Administration for the testing of the prototype deck for the Williamsburg Bridge. This testing of the deck at ATLSS was conducted by Research Engineer Mark R. Kaczinski, presently at The D.S. Brown Company in North Baltimore Ohio, and Research Assistant Peter Lugger, presently at Steinman Consulting Engineers in New York City. The deck sections were fabricated by Leonard Kunkin Associates of Lexington, PA.

7. References

1. Office for Research and Experiments (ORE) of the International Union of Railways, "Fatigue Calculations for Orthotropic Decks of Steel Railway Bridges", Report No. 5, ORE, Utrecht, April 1989.



2. A. Bruls, ed., "Measurements and Interpretation of Dynamic Loads in Bridges. Phase 3: Fatigue Behavior of Orthotropic Steel Decks. Common Synthesis Report", Commission of European Communities (ECSC), Directorate - General XII Science, Research and Development, March 1990.
3. American Association of State Highway and Transportation Officials Standard Specifications for Highway Bridges - LRFD, 1st Edition, 1994.
4. R.J. Connor, "Fatigue Criteria for Modular Expansion Joints", M.S. Thesis, Dept. of Civil and Environmental Engineering, Lehigh University, 1996.
5. M.R. Kaczinski, R.J. Dexter, and R.J. Connor, "Fatigue Design and Testing of Modular Bridge Expansion Joints", Proceedings of the Fourth World Congress on Joint Sealing and Bearing Systems for Concrete Structures, Sacramento, September 1996.
6. J.W. Fisher, R.J. Dexter, and M.R. Kaczinski, "Field and Laboratory Experiences with Expansion Joints", Structural Engineering in Consideration of Economy, Environment, and Energy, 15th Congress of IABSE, Copenhagen, Denmark, 16-20 June 1996.
7. R.J. Dexter, M.R. Kaczinski, and J.W. Fisher, "Fatigue Testing of Modular Expansion Joints for Bridges", IABSE Symposium San Francisco 1995, Extending the Lifespan of Structures, Vol. 73/2, pp.1091-1096, 1995.
8. J.A. Van Lund, M.R. Kaczinski, and R.J. Dexter, "Modular Bridge Expansion Joints for the Lacey V. Murrow Floating Bridge", 1997 Annual Transportation Research Board Meeting, Washington, D.C., January 1997.
9. Fisher, J.W., et al, Resistance of Welded Details Under Variable Amplitude Long-Life Fatigue Loading, National Cooperative Highway Research Program Report 354, Transportation Research Board, Washington, D.C., 1993.
10. Kaczinski, M.R., Dexter, R.J., and VanDien, J.P., Fatigue-resistant Design of Cantilevered Signal, Sign, and Light Supports, Final Report on Project 10-38, National Cooperative Highway Research Program, Transportation Research Board, Washington, D.C., 1996.
11. P. Grundy, Measurement and Interpretation of Strains on Westgate Bridge, Monash University Report, Australia, December 1990.
12. Kaczinski et al., "Full-Scale Fatigue Test of the Williamsburg Bridge Orthotropic Deck", Building an International Community of Structural Engineers, Vol. 1, Proceedings of Structures Congress XIV, Chicago, p.329, April 1996
13. R.B. Gajer, J. Patel and D. Khazem, "Orthotropic Steel Deck for the Williamsburg Bridge Reconstruction", Building an International Community of Structural Engineers, Vol. 1, Proceedings of Structures Congress XIV, Chicago, pp. 491-498, April 1996

Resistance of Open Stiffener Orthotropic Bridge Deck Plates according to the Eurocodes

Isabelle HEMERYCK

Assistant
University of Ghent
Ghent, Belgium

Isabelle Hemeryck, born 1971,
received her degree in civil
engineering from the University
of Ghent in 1995. She is
currently assistant at the
University of Ghent

Philippe VAN BOGAERT

Head of bridge design
TUC Rail
Brussels, Belgium

Philippe Van Bogaert, born 1951,
received his civil engineering
degree from Ghent University in
1974 and PhD in 1988. He is
currently head of bridge design
office with TUC Rail -Brussels
and professor at the Department of
Civil Engineering at
the University of Ghent

Summary

This paper presents the structural safety and fatigue safety verification of an existing orthotropic steel bridge deck, thus enabling a comparison of Belgian code and Eurocode requirements. Using the Eurocodes to verify the structural safety of a typical open structure orthotropic plated bridge deck, with non-continuous open stiffeners, is straight forward and is rarely determinant for this type of structure. The high concentrated loads of the traffic load model do not seem to introduce overestimated stresses. However, fatigue verification is more complex and requires extensive calculation. The paper compares results of the fatigue evaluation using the four Eurocode fatigue load models and shows that non-continuous stiffeners are highly fatigue-sensitive.

1. Introduction

The load models, as defined by Eurocode 1 (EC 1) part 3 for road bridges [1], are characterised by the absence of impact factors and the high magnitude of the concentrated loads. Both of these characteristics have a negative effect on the design of orthotropic steel plated bridge decks. In addition, recent studies [2] and [3] have demonstrated the high fatigue sensitivity of typical orthotropic plates. This sensitivity arises mainly at strip-butt welds and stress concentrations around cope holes in cross stiffeners. Furthermore, orthotropic deck plates can be analysed using either simple methods or with sophisticated computer programs. In any case, even current finite element models are unable to account for all possible structural details, for example cope holes. These must be analysed separately, thus overlooking their behaviour as a part of the whole structure.

For the above reasons, the Universities of Liège and Ghent, together with the national and regional authorities in Belgium, have started a research programme in order to study the EC 1.3 load models [4] and to evaluate the consequences of their introduction for existing bridges. Orthotropic steel plate bridge decks are the part of this programme being conducted by Ghent University.

2. Open stiffener deck plates

Bridge designers and owners are often alarmed by the complex behaviour of orthotropic plated bridges as well as results of tests on isolated cross beams which have shown that cope holes cause high stress concentrations and thus low fatigue strength. As a result, orthotropic plated bridges are rarely adopted. Therefore, within the joint research programme on the effects of EC 1.3, attention is given to various types of orthotropic plates. As a first step, a selection of



existing bridges with orthotropic plate has been made. All structures from this selection will be verified according to EC 1.3 and EC 2. This verification, together with thorough inspection, will eventually reveal if there is any problem at all. The existing structures were selected by considering the following important design parameters of orthotropic plates :

- open cross-section of bridge deck, with lateral girders or closed box section having shear diaphragms ;
- open or closed section longitudinal stiffeners ;
- longitudinal stiffeners welded between cross beam webs or continuing through cross beam webs with or without cope holes ;
- type of road surface, consisting either of several hydrocarbon layers (no special requirements) or of an extremely thin sheet of appropriate material.

The continuous box section girder of the overpass at Vilvoorde, having continuous closed section stiffeners, built in 1976 and supporting heavy road traffic, is presently being examined. The verification of the Gentpoort-bridge at Bruges, a small movable bridge deck of 16.15 m span built in 1977, has been completed. It consists of an open structure, having two main lateral girders, closely spaced cross-beams with depth about half that of the main girders and many light, non-continuous longitudinal I-stiffeners. The latter are connected to the cross beams by 5 mm fillet welds. This arrangement is shown in the cross-section of Figure 1. Figure 2 shows a photograph of the lower side of the structure. The structure was designed using the loading scheme of the Belgian code, approved in 1993. From [5] this code is certainly not severe, compared to the design loads of EC 1.3.

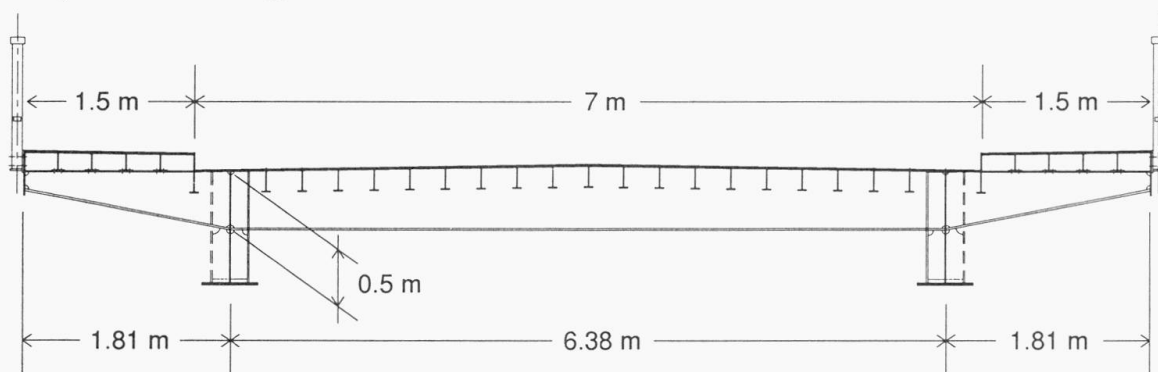


Fig. 1 Cross-section of the Gentpoort-bridge

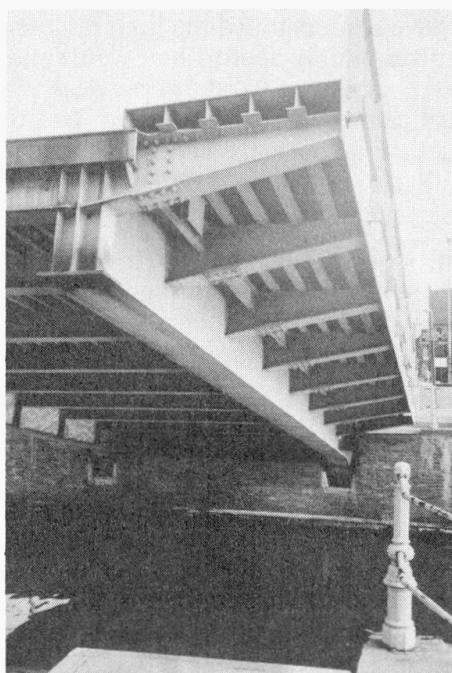


Fig. 2 Photograph of the lower side of the Gentpoort-bridge

The use of closely spaced open longitudinal stiffeners has a number of advantages. The deck plate is extremely light and is supported homogeneously. Compared to closed section stiffeners the number of longitudinal welds is double. However, thanks to modern automatic welding technique this does not affect the cost extremely. In addition the fatigue-sensitive cope holes in cross beam girders are left out. This has been adopted recently in important bridge constructions (Erasmus-bridge Rotterdam - Kronprinzen-bridge Berlin).

The road surface of the bridge being considered, consists of a thin sheet, glued to the steel structure. Hence there is no dispersal of concentrated loads through the pavement. This constitutes an unfavourable condition with respect to the effect of concentrated loads.

3. Structural safety

A full analysis, complying with the LM 1-scheme of EC 1.3, of the bridge deck being considered was carried out, using a fine mesh sophisticated FE-code (with Mindlin-elements) as well as by a current plane grid computer programme. The results of these calculations showed a rather good agreement. Figure 3 shows the deformation of the FE-model.

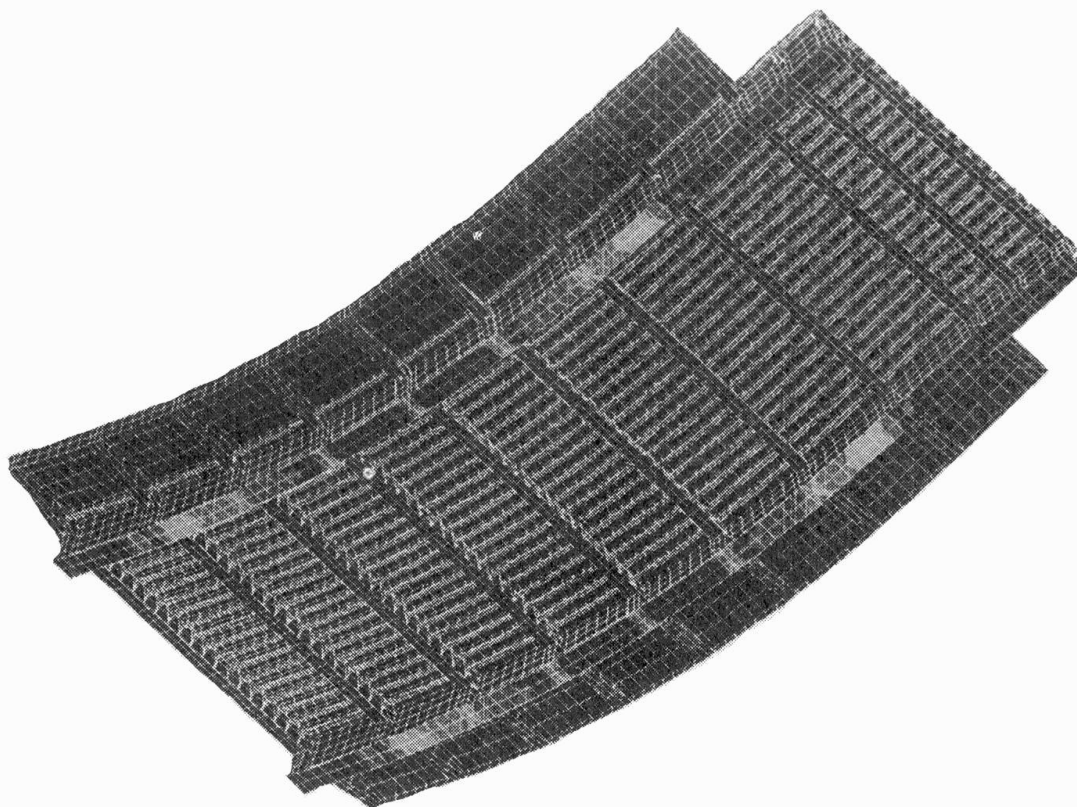
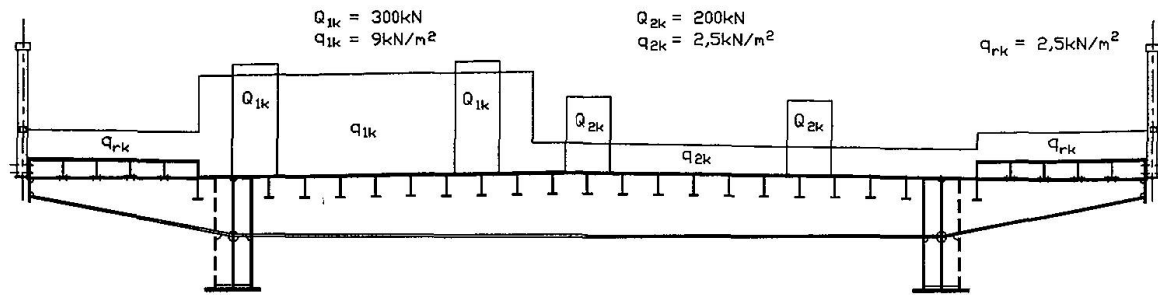


Fig. 3 Deformation of the FE-model

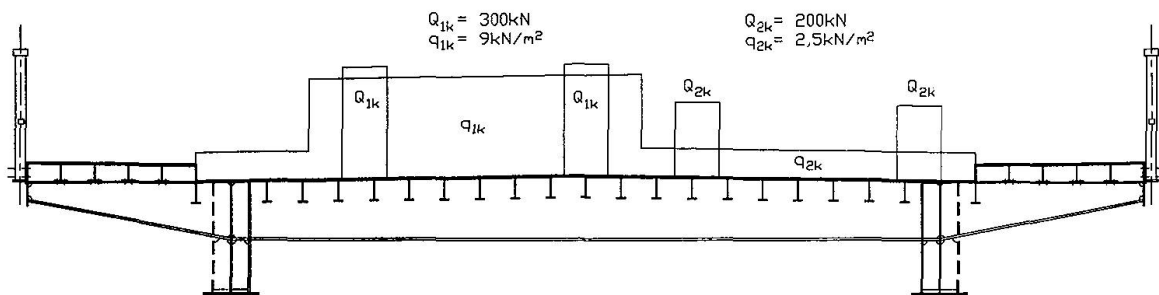
According to EC 1.3 there are 2 notional lanes, which must be located eccentrically on the bridge deck. Thus one main girder is loaded more heavily than the remaining one. Also, by placing the load model eccentrically, the cross beams and the longitudinal stiffeners can be loaded more heavily. Consequently the 5 positions, according to fig 4, across the bridge deck plate have been considered, whereas in fact real traffic is circulating in a less aggressive position. Similar positions were adopted for the LM 2-scheme.



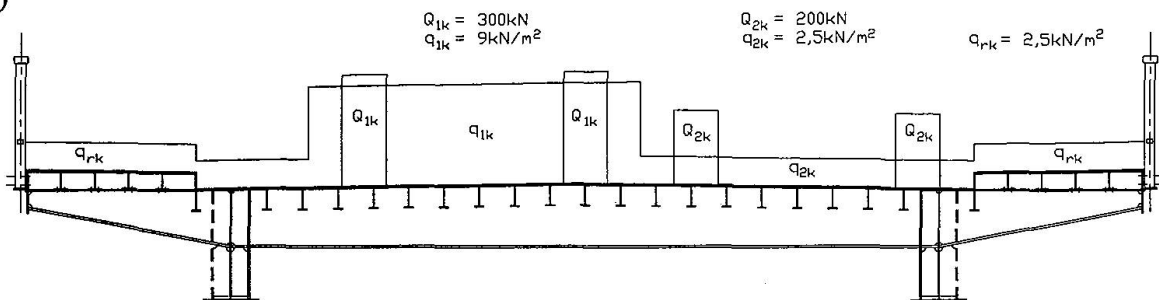
1)



2)



3)



4) : 2) with loading in 2 adjacent fields

5) : 2) with loading in 3 non-adjacent fields

Fig. 4 The 5 positions of traffic considered across the bridge deck

The verification of total stress at ULS, being far more easy than the use of actual strength criteria, Table 1 summarises the stresses which are the most relevant to the load carrying capacity. They include partial safety factors and dead load as well as the effect of the LM 1 and of LM 2.

stress ULS LM 1(Mpa)	stress ULS LM 2(Mpa)	location	direction to bridge deck axis	at cross section
$f_1 = 297$	$f_1 = 144$	lower flange lateral main girder	parallel	near mid-span
$f_2 = 201$	$f_2 = 134$	lower flange cross beam	perpendicular	near mid-span
$f_3 = 241$	$f_3 = 183$	lower flange long stiffener	parallel	near mid-span
$f_4 = 214$	$f_4 = 165$	principal stress long stiffener to cross beam	parallel	near 1/4 of bridge length

Table 1 Total stress at ULS

As expected the bending stresses in the different elements - main girders, cross beams and stiffeners - are the representative figures, together with the principal stress at the joint of stiffener and cross beam. In Figure 5 a detail of this joint is given. The reader will take notice of the cut-outs avoiding triaxial welds. These cut-outs introduce stress concentrations, which generate the altogether not too large stresses f_4 . Anyway, in spite of the low value of the initial design loads, this construction satisfies all criteria for structural safety, the most relevant being the main girder stresses.

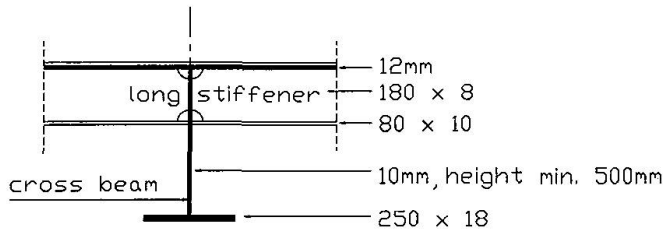


Fig. 5 Joint of stiffener and cross beam

4. Fatigue resistance

The tools for verifying fatigue resistance are similar to those for checking structural safety. However, this verification is far more complex. Instead of comparing total stresses to a single value of f_d , stress ranges at various fatigue-sensitive points must be compared to category-values defined in the tables of EC 3.1-9 [6]. Furthermore, 4 load models, some consisting of many vehicles must be considered. Taking into account the various fatigue details, more than 9 locations were analysed, as shown in Figure 6 and listed in Table 2.

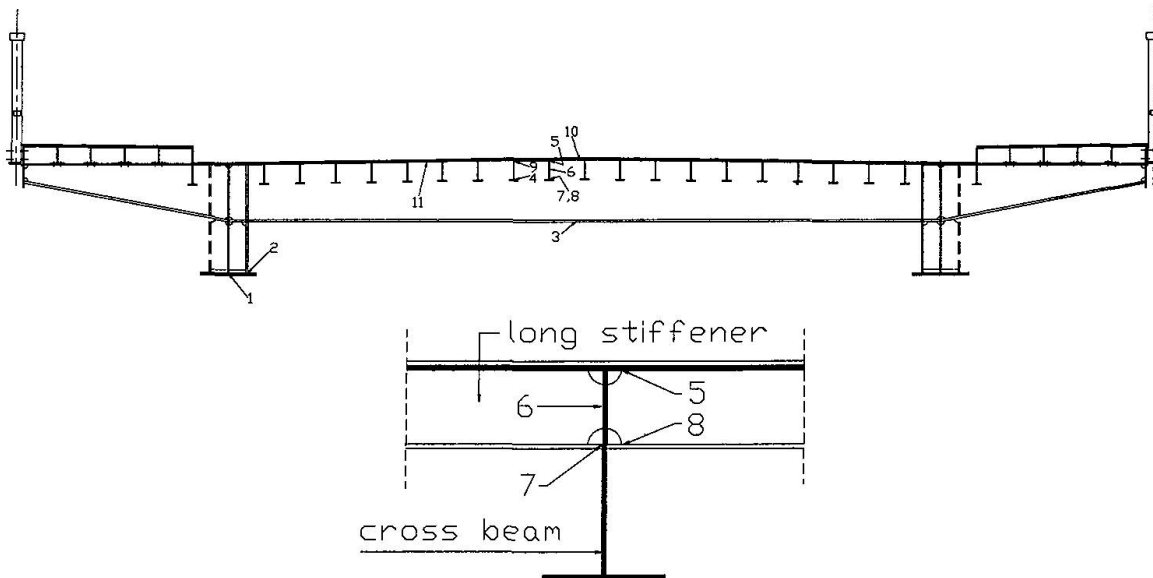


Fig. 6 Points considered for verifying fatigue resistance



Location	Fatigue detail	Category
1	lower flange welded main girder	112
2	main girder where connected to vertical stiffener	71
3	lower flange welded cross beam	112
4	lower flange welded stiffener in between cross beams	112
5	weld cutout stiffener to cross beam web near upper flange	71
6	fillet weld stiffener web to cross beam web (shear)	80
7	fillet weld lower flange stiffener to cross beam	45
8	weld cutout stiffener to cross beam web near lower flange	71
9	stiffener web welding to deck plate in between cross beams	112
10	cross beam web welding to deck plate	80
11	bending in between stiffeners of butt weld in deck plate	71

Table 2 Points considered for verifying fatigue resistance

The verification of fatigue resistance first requires a comparison of the constant amplitude ($5 \cdot 10^6$ cycles) category value $\Delta\sigma_D$ to the stress ranges due to fatigue load models 1 and 2 (FLM1 and FLM2). Then, fatigue safety is represented by the following inequality :

$$\Delta\sigma_{\text{FLM1 or FLM2}} \leq \frac{\Delta\sigma_D}{1.15} \quad (1)$$

If Equation (1) is satisfied, there is no fatigue damage for the given detail. The use of FLM1 has no special requirements. FLM2 however, consists of 5 lorries. It is not evident which lorry is determinant and the effects of the lorries are only slightly different. Since the main girders have a span of less than 20 m lorry 3 can be expected be determinant for these elements, whereas lorries 2 and 4 are determinant for the 1.9 m spaced cross beams and stiffeners. Table 3 summarises the effects of FLM1 and FLM2 and also indicates which lorry is determinant. The value of $\Delta\sigma_D$ is given for each case and the stress ranges which do not meet the criterion of Equation (1) are boxed.

Point	1	2	3	4	5	6 ($\Delta\tau$)	7	8	9	10	11
$\Delta\sigma_{\text{FLM1}}$	120.1	107.5	88.4	126.8	64.6	33.3	82.7	106.9	82.7	35.7	92.9
$\Delta\sigma_{\text{FLM2}}$	62.2	59.7	42.0	111.4	34.6	22.3	64.1	75.1	42.3	15.0	31.5
Lorry	3	3	2	1	2	4	2	2	4	4	4
$\Delta\sigma_D$	82.5	52.3	82.5	82.5	52.3	66.6	33.2	52.3	82.5	58.9	52.3

Table 3 Stress ranges introduced by FLM1 and FLM2 ($\Delta\sigma$ in MPa)

This results agree in general with those found in the literature. FLM1 is less aggressive than FLM2. In addition, for this particular case the results of FLM2 require closer verification on the main girders as well as on the longitudinal stiffeners, the latter both at its ends and at mid-span. The next step is the use of FLM3 and FLM4 for determining the structure's life-time. Stress ranges

$\Delta\sigma_{\text{FLM3}}$ due to FLM3 are easily found, whereas $\Delta\sigma_{\text{FLM4}}$ must be determined from the effects $\Delta\sigma_{i,i=1,5}$ of 5 lorries, each occurring with a percentage f_i according to the traffic type. Consequently $\Delta\sigma_{\text{FLM4}}$ is found from [7]

$$\Delta\sigma_{\text{FLM4}} = \left(\sum_{i=1}^5 Ds_i^5 f_i \right)^{0.2} \quad (2)$$

whereas the structure's life-time, according to the fatigue detail being considered, is found from

$$\text{life-time} = 100 \text{ years} \frac{5 \cdot 10^6 \left(\frac{\Delta\sigma_D}{\Delta\sigma_{LM}} \right)^5}{N_{\text{obs}} 0.67 k_2} \quad (3)$$

N_{obs} (number of lorries per 100 year per slow lane) equals $200 \cdot 10^6$ for road category 1, $50 \cdot 10^6$ for category 2, $12.5 \cdot 10^6$ for category 3, although the denominator of this expression must be lower than $100 \cdot 10^6$. The aim is to find the road category which corresponds to a life-time of at least 100 years. The calculation results with FLM3 and FLM4 are summarised in Table 4.

Point	1	2	3	4	5	6	7	8	9	10	11
$\Delta\sigma_{\text{FLM3}}$	59.6	51.7	37.1	82.7	41.2	24.9	52.95	67.8	30.9	11.0	25.3
life FLM3 cat 1	25.3	5.3	272	5	16.5	684	0.5	1.4	682	22008	189
life FLM3 cat 2	75.7	15.8	661	5.5	18.2	755	0.5	1.5	752	53542	563
life FLM3 cat 3	303	63	2646	21.9	72.8	3021	2.1	6	3009	∞	2254
$\Delta\sigma_{\text{FLM4 type1}}$	43.5	42.2	29.1	79.7	24.3	16.2	37.4	44.7	30.0	10.7	21.2
$\Delta\sigma_{\text{FLM4 type 2}}$	39.9	38.8	26.7	79.1	23.7	16.0	35.8	43.3	29.1	9.7	21.3
$\Delta\sigma_{\text{FLM4 type 3}}$	35.5	34.6	24.1	78.8	23.1	15.9	34.4	42.1	28.3	8.4	21.4
life FLM4 type1 cat 1	122	14.6	923	6	230	5825	2.7	11	781	25755	459
life FLM4 type2 cat 2	562	66.5	3405	6.8	289	6845	3.8	14.2	1003	∞	1333
life FLM4 type3 cat 3	4057	471	23090	28	1312	28726	18.5	65	4681	∞	5224

Table 4 Calculation results with FLM3 and FLM4 ($\Delta\sigma$ in MPa)

Again in Table 4 the boxed values do not comply with the requirement of 100 years life-time. FLM3 appears too conservative for details 2 and 5. Hence in this case the use of FLM4 is more accurate for the main girder. From the design loading of this bridge, the structure should match the conditions for local traffic and road category 3. However due to stress ranges in details 4, 7 and 8 the structure doesn't even comply for FLM4 and road category 3. Clearly this is due to the severity of the fatigue category-values of these details.

After observing the number of lorries crossing the bridge, which consists of only one lane, the daily average N_{obsj} is 60 lorries, so N_{obs} equals

$$0.9 \times 365 N_{\text{obsj}} \times 100 \text{ years} = 1.971 \cdot 10^6 \text{ for observed category 4} \quad (4)$$

In these conditions, the life-time for FLM3 and FLM4 for road category 4 take the values from Table 5.

Point	1	2	3	4	5	6	7	8	9	10	11
life FLM3 cat 4	1919	400	16779	139	461	19161	13.6	38.2	19082	∞	14293
life FLM4 type3 cat 4	25728	2988	∞	176	8318	∞	117.5	412	29685	∞	33132

Table 5 Calculation results with FLM3 and FLM4 for observed category 4

We can see that FLM3 is too conservative for details 7 and 8. For FLM4 all details comply with the requirement of 100 years life.



According to FLM2 detail 2 has a limited life-time if intensive lorry traffic is considered, where FLM4 is more accurate. FLM2 as well as FLM4 predict the reduced fatigue resistance of the points 4, 7 and 8. Thus the calculation for all lorries of the bridge is necessary. This is a tedious operation, requiring special effort of the designer and high calculation cost. In addition, from this example it is shown that fatigue assessment is no longer a verification, but becomes a determining criterion. Concerning the bridge being verified, it satisfies all requirements for local traffic and the observed category 4. Inspection should be concentrated on the joints of longitudinal and transverse stiffeners and on the lower flange of the longitudinal stiffener. As expected, the use of non-continuous longitudinal stiffeners, welded in-between cross beams, reduces fatigue resistance.

5. Conclusions

From the detailed verification of the Gentpoort-bridge it was implied that structural safety, according to Eurocodes 1 and 2 is not determinant for open stiffener orthotropic bridge deck plates. On the other hand, the application of the load models for fatigue resistance and assessment shows that extensive calculations are needed. Furthermore, details showing fatigue damage according to FLM2, cause no problems according to FLM4. This proves that the complete application of EC 1.3 is imperative, thus increasing design cost. For a small bridge FLM2 seems more accurate than FLM1. While verifying the structure's life-time it was found that fatigue assessment by FLM4 is more accurate than FLM3.

References

1. EC 1.3.
2. LEHRKE, H.P. Fatigue design of orthotropic steel decks of road bridges - Measurements and interpretation of dynamic loads on bridges, Report Fraunhofer Institut Darmstadt, March 1995.
3. MANG, F.; BUCAK Ö.; Karcher, D. New developments on orthotropic steel bridge decks: fatigue tests, E & FN Spon, 1996.
4. BRULS, A.; LABEEUW, G.; VAN BOGAERT, Ph. Procedure developed in Belgium for the evaluation of existing steel bridges., IABSE Workshop Evaluation of existing steel bridges, Lausanne 1997.
5. JACOB, B. - PRAT, M. Étude du trafic routier sur les ponts. Calcul des sollicitations et comparaison de différents règlements des charges, AITBTP no 482, Mars-avril 1990 pp 89-118.
6. EC 3.1 Chapter 9.
7. BRULS, A. Résistance des ponts soumis au trafic routier. Modélisation des charges - Réévaluation des ouvrages., PhD-thesis Université de Liège, 1995.

Fatigue Assessment of Steel Bridges of the Bullet Train System

Chitoshi MIKI

Professor
Tokyo Inst. Of Technology
Tokyo, Japan

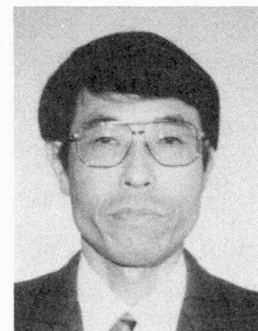
Chitoshi Miki, born in 1947, got his civil engineering degree at Tokyo Institute of Technology. His main fields of research are fatigue and fracture of welded structures, fracture mechanics and bridge maintenance.



Atsushi ICHIKAWA

Chief Engineer
Railway Techn. Res. Inst.
Tokyo, Japan

Atsushi Ichikawa, born in 1952, got his masters degree at Tokyo Institute of Technology. He has been engaged in bridge engineering works.



Summary

It is over 30 years since the first bullet train system was opened for public service in Japan. The structures of bullet train systems have been supporting the operation without any accident. But they have been showing signs of deterioration. This paper is intended to give an outline of fatigue problems in regard to assessment and life extension works in steel bridges of bullet train systems.

1. Introduction

The bullet train systems are the most important trunk lines in Japan. For example, the Tokaido Shinkansen, the first bullet train system completed in 1964, covers a distance of 515 km between Tokyo and Osaka. Nearly 250 trains run daily at the maximum operating speed of 270 km/h. The daily passenger traffic reaches as high as 300 thousands.

The structures of bullet train systems have been supporting the operation without any fatal accident. But they are showing some signs of deterioration. In particular, the fatigue damage in welding joints of steel bridges attract our close attention [1]. However, no fatal accidents have taken place yet because inspections of these bridges have been routinely carried out, and fatigue cracks discovered were properly repaired. Fatigue damage have developed only in the secondary members not incorporating any fatigue design.

Hereafter, there will be a greater demand for increasing the train speed and increasing the transportation capacity, therefore researches for upgrading the structural details efficiently and reliable maintenance are required necessarily.

2. Outline of Steel Bridges in Bullet Train Systems

2.1 Bridge Structures

Plate girder, truss girder and composite girder bridges have been usually used in the bullet train systems. With regard to the track structure, open floor track with a small dead load is in use for many of steel bridges in the early bullet train system in consideration of economy, because the noise in that type of bridge did not cause any social problem in the construction period. The open floor track is not applied now to the steel bridges in the area where the noise becomes a problem, and the ballasted track or concrete slab track is applied. And the noise insulating devices were attached to most of open floor type steel bridges in the bullet train system in the latter half of 1960's.



2.2 Standardization of Design of Structural Details

Standardization of the design has been introduced for the structures of bullet train systems as much as possible, because in the construction of structures it is required to attain the maximum economy. Therefore, similar structural details were adopted for the same type of bridge, and this is to be considered for maintenance. With regard to the welding joints, the welding was really applied to the steel bridges at the same time in construction of structures of the first bullet train system. Some of the details of welding joints have been improved, not being applied at present.

2.3 Fatigue Design History

The first codes for the fatigue design of railway welded steel bridges had been established in 1956, being strongly influenced by DIN of the day especially with regard to welding joints. The allowable fatigue stresses had been set up based on fatigue strengths at two million cycles which were considered as fatigue limits.

Fatigue design for the Tokaido Shinkansen system was done based on codes established in 1960, in which the results of fatigue tests which had been carried out in Japan were taken up and the allowable fatigue stresses related to 500 MPa class steel were added. And a consideration was made such as setting design fatigue train load at 18 tons against design train load of 16 tons with the aim of reflecting the difference in influence line length on number of design stress repetitions. On the other hand, for the subsequent bullet train system, the design fatigue train load was set at 19 tons, the increasing train load being considered.

The allowable fatigue stresses were revised in 1970, based on fatigue strengths in non-destructive probability of 95 %. Furthermore, in the design codes established in 1972 for Tohoku and Jyoetsu Shinkansen which are the bullet train systems opened in 1982, the design life of 70 years was set up and stress repetitions during the life were considered in the allowable fatigue stresses.

In 1983, the fatigue design codes were revised with reference to the large scale fatigue tests and other results.

The current fatigue design codes were revised in 1992 reflecting the latest results.

2.4 Changes in Circumstances of Service Conditions

The service conditions have been changing from the opening to the present state. Not only the volume of traffic but also the train speed is increasing. These have all changed in the direction of increased severity for structures. In regard with the train speed the maximum speed has been increasingly changing from 210km/h to 270km/h. However, the weight of vehicle is changing lightly in consideration of effect on the structures. The axle load of vehicle with the maximum speed of 220 km/h (car type A) is about 150 kN and that with the maximum speed of 270 km/h (car type B) is about 110 kN.

In these circumstances, some phenomena are observed such as an increasing out-of-plane vibration of web plate. Fig.1 shows the relationship between the train speed and the stress of flange plate in the deck plate girder, and between the speed and out-of-plane acceleration of web plate. Stresses considered in the design stage such as flange plate stress are closely related to vehicle weight rather than train speed, but the out-of-plane vibration is much increasing with train speed.

3. Observed Fatigue Damage and Retrofitting Works

3.1 Outline of Observed Fatigue Damage

The structures of bullet train systems suffered from very severe loading condition caused by high-speed train operation and highly repetitive frequencies.

Concerning steel bridges, several types of fatigue damage have been observed as shown in Fig.2[2][3]. These types of damage began to be observed in about 8 years after the opening of service. Some types of fatigue cracks are comparatively rare in the conventional railway system. They are in many cases caused by stress concentrations due to structural details of members, by out-of-plane displacements occurring between perpendicularly crossing members

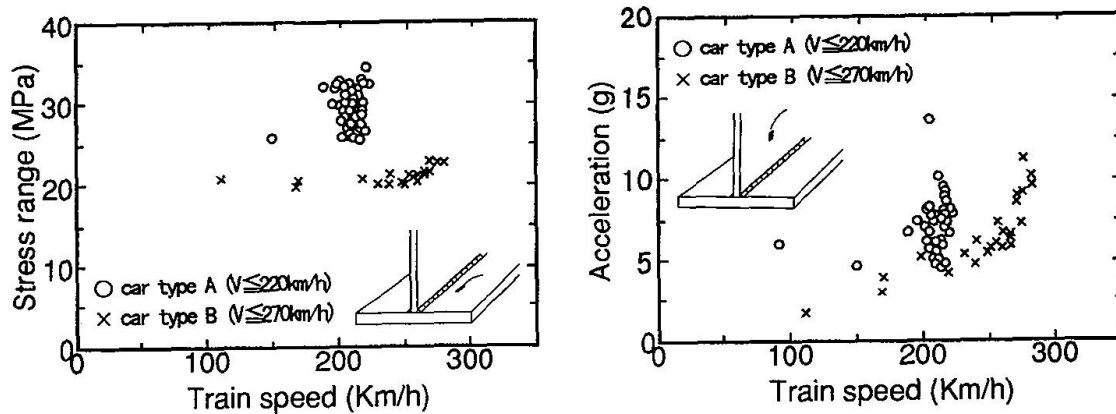


Fig.1 Relationship between train speed and stress range of flange or acceleration of web

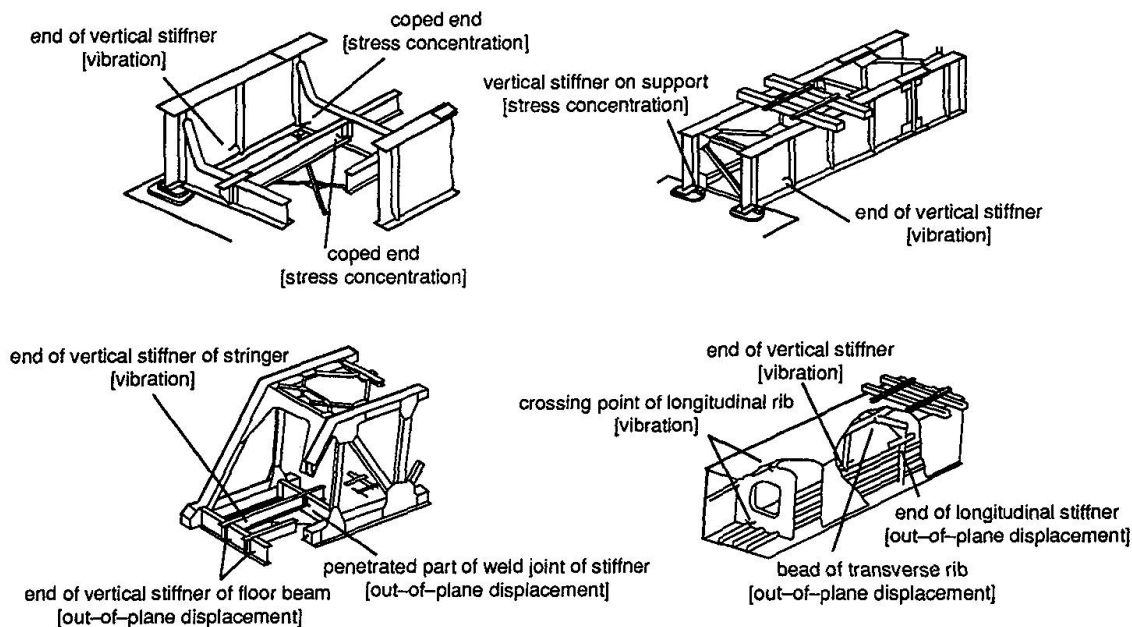


Fig.2 Fatigue damage in steel bridges

such as main girders and cross beams or cross beams and stringers, and by vibration due to distortion under high-speed operation of trains peculiar to bullet train system.

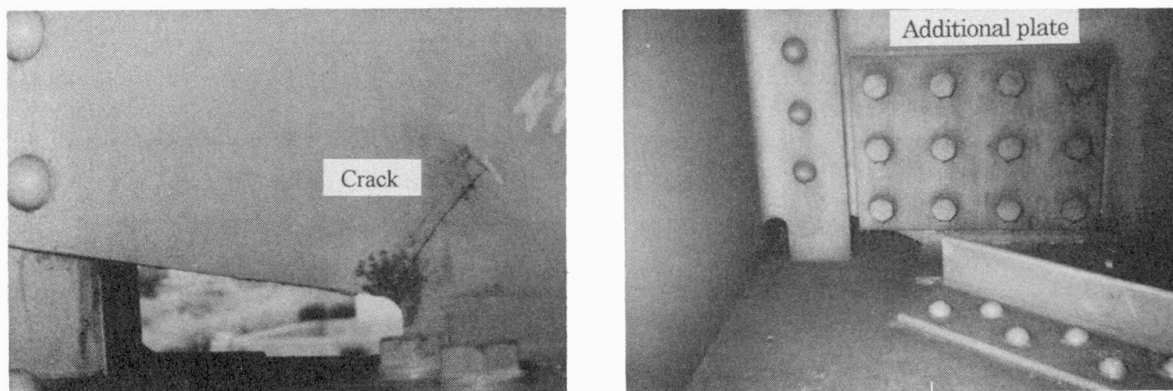
A fatigue crack has not yet been detected at important portion of main members which lead to catastrophic failure where fatigue was assessed in the design stage. Fatigue cracks are, however, often discovered at such as secondary members as side walks, connections of attached facilities and diaphragms or secondary local portions of the main members. These types of damage were already repaired and almost of details which had the possibility of occurrence of the same kind of damage were also retrofitted.

3.2 Coped Cross Beam of Through Plate Girder

The damage was observed at the coped end of the web plate of cross beam, as shown in **Fig.3**. Many cases of damage were observed in end cross beams. The crack usually develops obliquely from the corner of coped end of web plate to the inside of web plate. This type of damage was discovered in about 8 years after the opening of service.

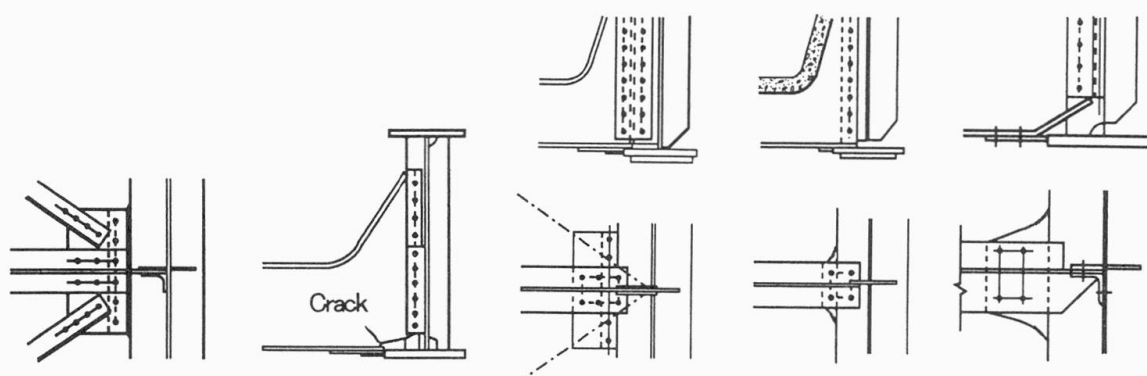
Measurements of actual bridges, structural analysis and fatigue tests were carried out in order to study causes and retrofiting methods. The results are as follows;

(1) The main cause of this fatigue crack was that the end of lower flange of the cross beam was



(a) Crack

(b) Retrofitting method

Fig.3 Damage and retrofitting of coped cross beam

(a) Original detail

(b) Improved detail

Fig.4 Improvement of details of cross beam

coped to connect with main girder and this induced stress concentration.

(2) The measured stress becomes higher in the case of normal shoe seat than in the case of damaged shoe seat. Thus, the settlement of supporting point was also one of the causes.

(3) In the retrofitting, additional plates were applied to web plate in order to increase the loading capacity. A sufficient reinforcing effect was obtained.

(4) The details of the currently designed bridge was improved as shown in **Fig.4**

3.3 Coped Stringer of Open floor Type Bridge

A crack occurred at the stringer web plate of through plate girder or through truss, as shown in **Fig.5**. This type of crack was discovered in about 10 years after the opening of service.

The stringer is a member which is directly subjected to the train load, and to the great lateral force and impact by high speed train. It is necessary to avoid a local stress concentration by improving the lateral rigidity or keeping the stress flow as continuous as possible. However, in some bridges the lower flanges of stringer were not connected to the cross beam. This caused the stress concentration at the cope combined with it and led to cracking.

With regard to the repair, the lower flange was connected with the cross beam web plate by extending it to the stringer end.

3.4 Intermediate Diaphragm in Box Section Deck Plate Girder

In the box section deck plate girder, intermediate diaphragms are provided at intervals of 5 to 6 m in order to improve the torsional rigidity. Diaphragms are connected by welding with flange plates or longitudinal ribs. Fatigue cracks were observed at this detail, on the surface of diaphragm at the toe of fillet weld, as shown in **Fig.6**.

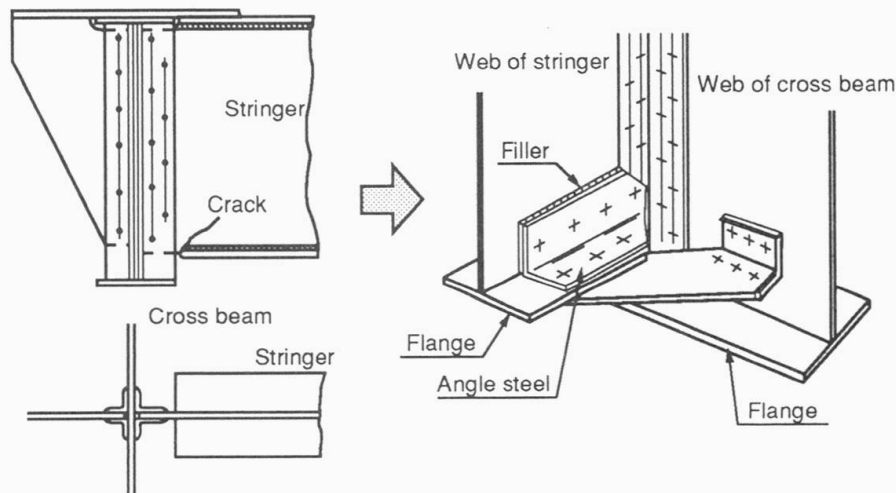


Fig.5 Damage of coped stringer

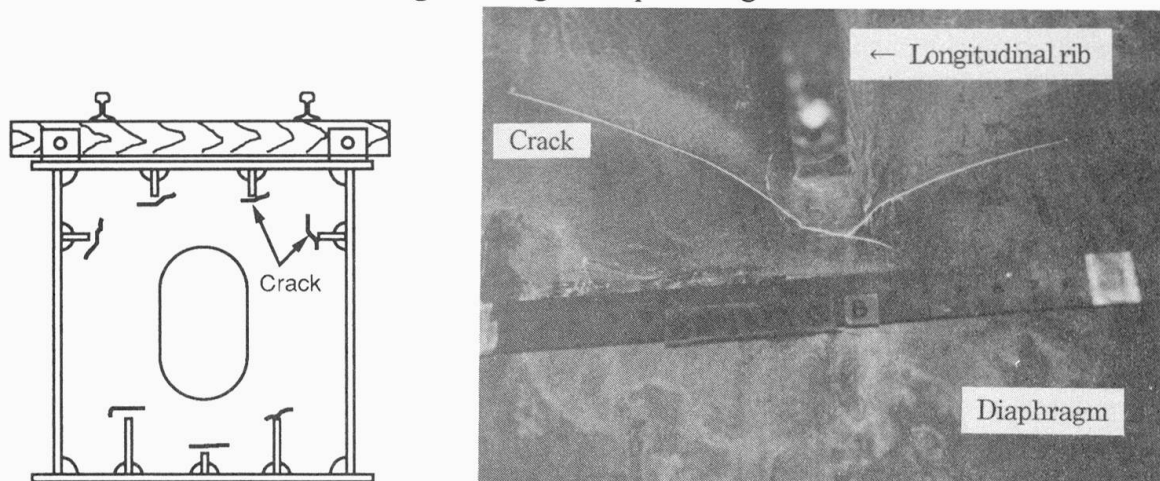


Fig.6 Damage of intermediate diaphragm

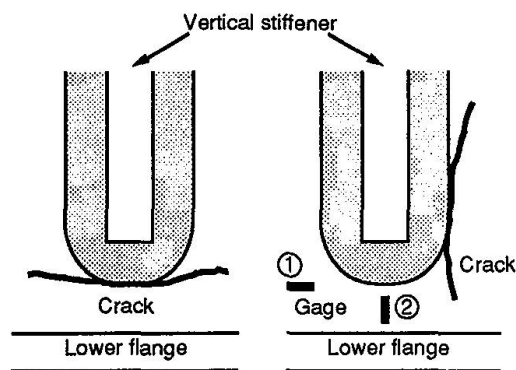
This type of crack is caused mainly by the stress concentration at the toe of weld and the high structural constraint. Diaphragms with such a structural detail are affected by an out-of-plane vibration with the passage of a high speed train and subjected to considerable fatigue at the restrained weld.

This damage was repaired by drilling a stop hole at the crack tip, or rewelding after gouging and the tungsten inert gas arc remelting (TIG-melting) applied at the toe of fillet welds.

3.5 End of Vertical Stiffener in Web Plate

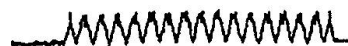
Many fatigue cracks were observed at the lower ends of the vertical stiffeners attached to the web plates of stringers of truss girders or box-section deck girders. This type of fatigue damage was discovered in about 10 years after the opening of service, being hardly observed in the bridges in the conventional railway systems. The crack originates primarily at the toe or the root of fillet weld around the lower end of the vertical stiffener and develops horizontally into the base metal of the web plate. Such a crack may sometimes propagate along the weld toe, and progress in the direction horizontal to the base metal with some length. On the other hand, in the fatigue tests of beam specimen under in-plane bending, cracks usually progress in the perpendicular direction along the toe of weld as cruciform joints. These are shown in Fig.7.

Fig.8 shows a comparison between the in-plane stress histories along the bridge axle of lower end of stiffener and out-of-plane bending stress histories of that. This shows that the former waveform is almost the same as anticipated in the design, while the component of vibration is contained in the latter waveform. Thus, It seems that this type of crack in the actual bridge is caused mainly by the increasing of out-of-plane vibration on web plate due to deflection of



(a) Actual bridge (b) Fatigue test
Fig.7 Progress of crack

① Plane stress waveform along bridge axle



② Out-of-plan bending stress waveform perpendicular to bridge axle



Note : For the position of strain gage at the time of stress measurement, see Fig.7.①②

Fig.8 Stress histories of end of vertical stiffener

sleepers and those due to distortion induced by a high speed operation of trains, in addition to the plane stress in the design [4].

This damage is repaired by applying additional plates to the web plate in order to prevent the deformation after gouging and rewelding, and furthermore, applying the TIG-melting at the toe of fillet welds. This type of fatigue damage is, however, increasing and there are many more points likely to suffer such damage.

3.6 End corner of girder reducing section

Regarding the through plate girder and the deck plate girder, there is a type of reducing the height of girder near the bearing. As shown in Fig.9, a crack has been observed along the weld at the corner since several years ago[5]. It was revealed that the stress components perpendicular to the weld bead is superior. The small radius of the corner, groove weld with full penetration not being used, and out-of-plane vibration due to the high speed train operation are conducive.

This damage was repaired by applying additional plates to the web plate in order to decrease the stress after gouging and rewelding the fatigue crack.

3.7 Sole Plate of Box Section Deck Plate Girder

A sole plate is usually attached to the lower flange plate with high strength bolts in railway bridges, but in the box section plate girders of long span, fillet welding is used together with bolt joint.

A crack has been observed since several years ago, as shown Fig.10. This crack is observed on both the transverse welds and the longitudinal welds. The crack initiates from the root of weld, propagates along the bead of weld, and enters the lower flange plate [6]. Stress measurements of actual bridges, structural analysis and fatigue tests were carried out in order to study causes and retrofitting methods. The results are as follows;

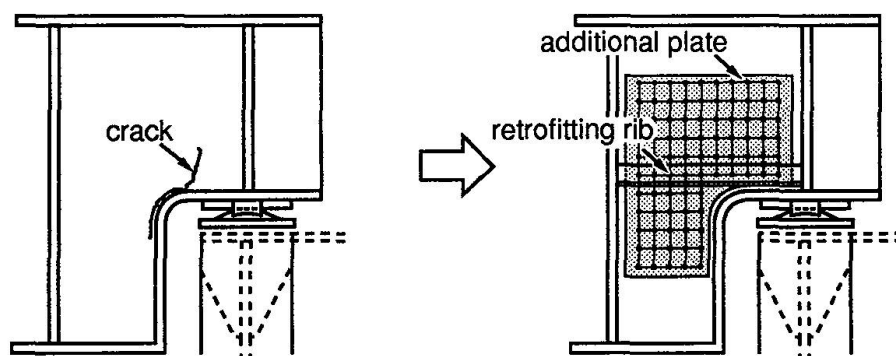


Fig.9 Damage of end corner of girder reducing section

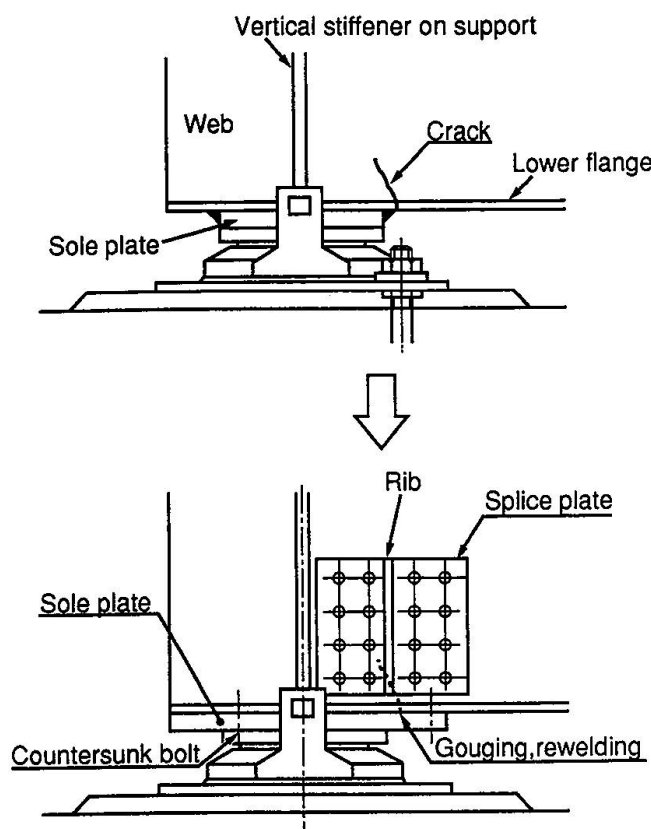


Fig.10 Damage of sole plate

(1) A poor condition of movable bearing increases the stress around the sole plate.

(2) A gap between the sole plate and the flange plate increases the stress.

(3) In the retrofitting, a function of movable bearing must be improved, and sufficient reinforcing effect is obtained by exchanging the sole plate for a new one with bigger size after gouging and rewelding the crack.

4. Damage Prevention Works

4.1 Outline of Prevention Works

Inspections of railway structures consist of periodic regular inspection which is arrived out every two years and individual special investigation which is done when any damage is detected during a periodic inspection. The inspection is made by qualified engineers of railway company which manages and operates the line. These engineers have thorough knowledge about fatigue and corrosion which occur in bridge structures, and possess the capability of carrying out stress measurements,

nondestructive test, etc. However, with regard to new type of damage, causes and retrofitting methods are usually studied by the advisory committee consisting of specialists including university professors. Damage prevention works are considered based on these inspections and advice. Fig.11 shows an outline of prevention works. The aims of prevention works are mainly as follows;

- (1) To find the checking points of details.
- (2) To presume the possibility of fatal fatigue damage and new type of damage.
- (3) To recommend a method of repairing such damage.

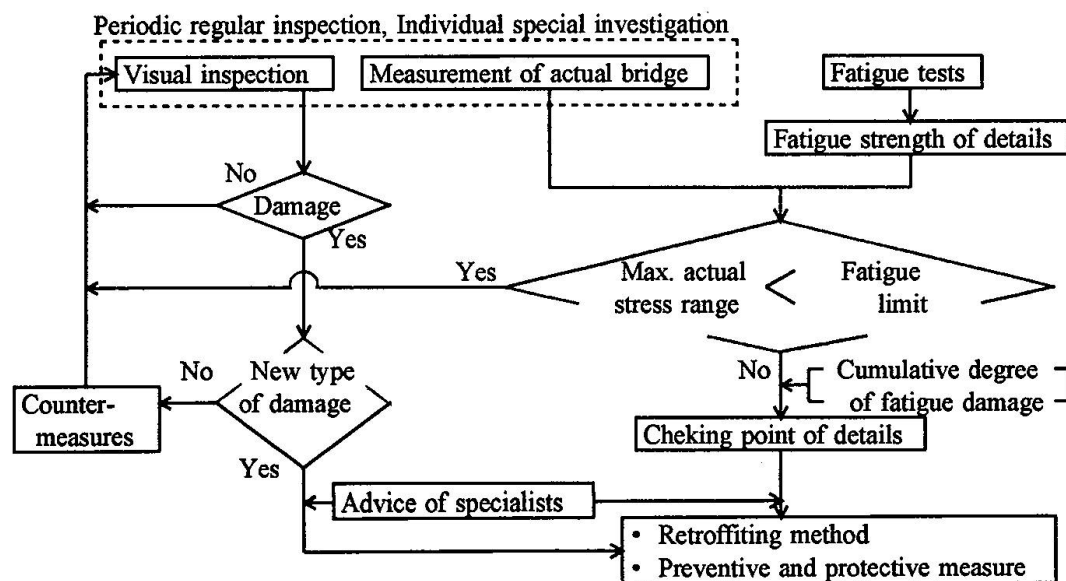


Fig.11 Outline of prevention works



Because most of structural details in steel bridges were standardized, it is likely that similar damage occur at certain points when a certain type of fatigue damage occurs. A more rational maintenance program is an important subject to cope with this serious problem.

When what had been assumed at the time of designing and the subsequent condition of use are considered, certain parts in bridge structures are approaching the ends of their design service lives in calculation. Therefore a number of preventive and protective measures against fatigue damage have been considered. One of these measures is the TIG-melting applied at the toe of fillet welds of lower ends of vertical stiffeners and at the toe of welds on the surfaces of diaphragms. This measure was done about 8 years ago, being applied to all of the box section deck plate girders with ballastless track.

4.2 Damage Checking Points in Prevention Works

One of main prevention works is to determine the fatigue strengths of structural details used in the actual steel bridges. However, fatigue strengths should be determined under the higher repetitions of thousands of loading on railway bridges. Thus, many higher repetitive fatigue tests have been carried out. I-shaped test pieces with various joints such as Fig.12 were used in these fatigue tests. Results of these fatigue tests are reflected in the current design codes.

What have greatly changed in allowable fatigue strengths between the former design codes and the current design codes are longitudinal welds between flanges and webs, ends of gusset plates welded to webs, ends of gusset plates welded to flanges, ends of vertical stiffeners, and fillet welds between sleeper pads and flanges, shown in Fig.13. They are the major checking points in the prevention works.

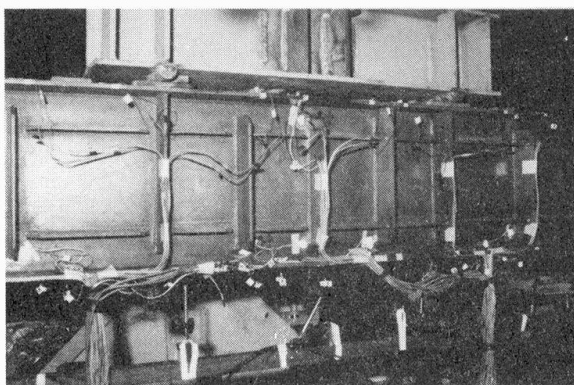


Fig.12 Fatigue test specimen

4.3 Measurement of Actual Bridges

Another important preventive work is to grasp the degree of fatigue damage based on stress measurements in actual bridges. It is thought to consider maintenance based on stresses actually occurring in bridge members, since actual stresses are normally low compared with those in design calculations, measured stresses of the same type bridges show wide differences, and stresses not to be considered in the design such as out-of-plane stress of web plate are measured in some details. The reason for actual stresses being low compared with calculated stresses in case of railway bridges, lies in the load distribution due to rails and secondary members.

Stress measurements consist of grasping the maximum nominal stress range occurring in the detail (Fig.14) for comparison with the fatigue limit and the cumulative degree of fatigue damage.

The rain flow counting method is used to obtain stress range histograms from stress records, and the equivalent stress range and the cumulative degree of fatigue damage are calculated by applying the Miners law.

Many of bridges should be measured with priority, and in the measurements the following points should be considered in deciding the priority of bridges. This is also similar to bridges in the conventional railway system.

- (1) Open floor type bridges are apt to be subjected to effect of fatigue, on account of large stress range.
- (2) Short span bridges are apt to be subjected to effect of fatigue, on account of repetitive loading.

4.4 Estimation of Steel Bridges

Fig.15 shows the results of stress measurements in actual bridges [7]. Measured stress range is very small in comparison with calculated one, as described in 4.3. This shows clearly that high possibility of fatigue damage in a fairly large number of members is found on the basis of design calculated stress, but there is hardly any cause as far as actual stress is concerned [8].

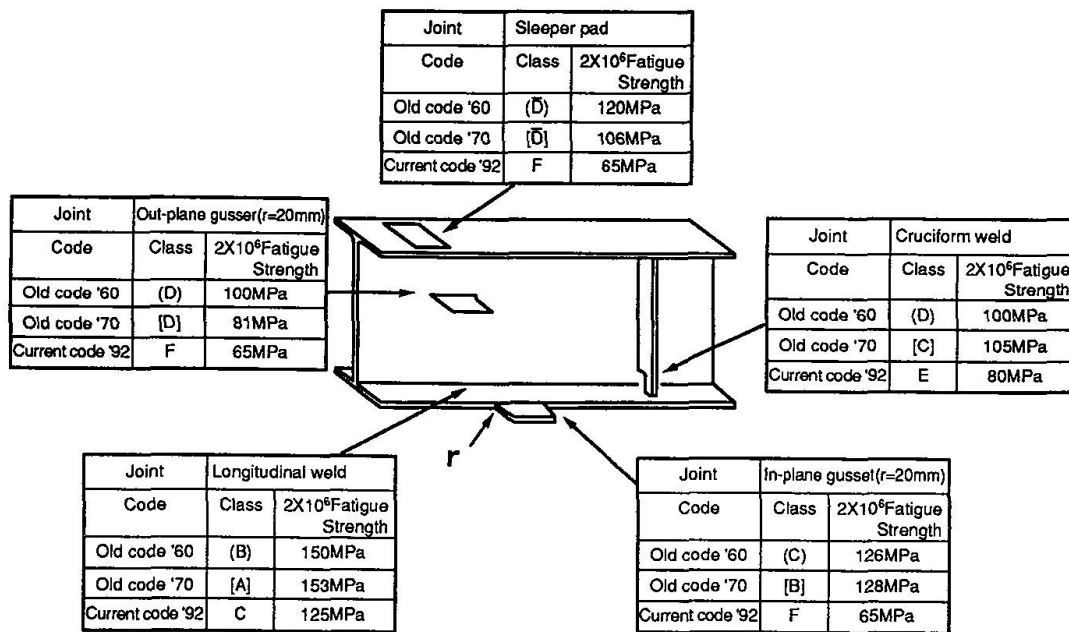


Fig.13 Changes of allowable fatigue stresses in design codes

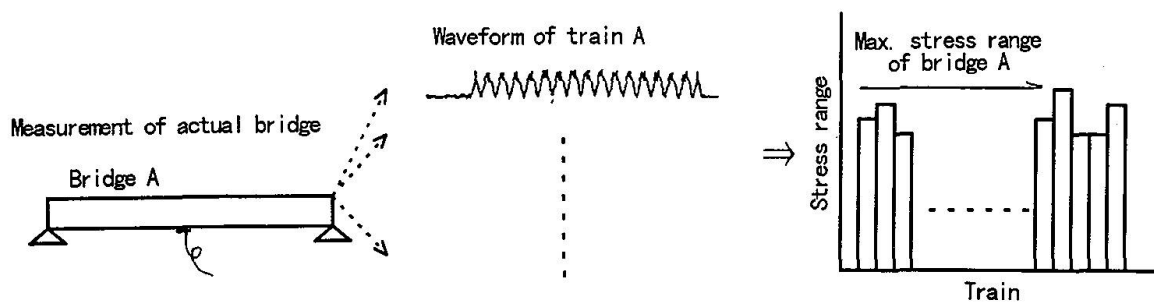


Fig.14 Maximum stress range of a bridge

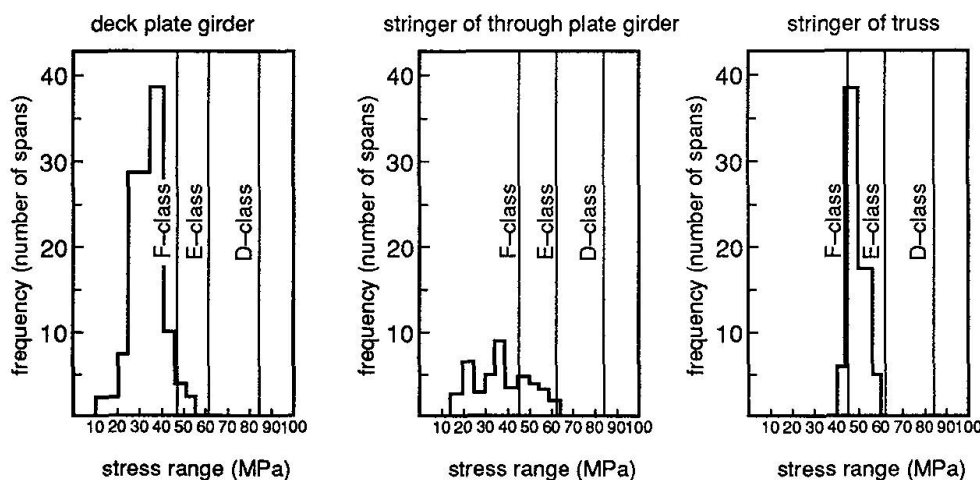


Fig.15 Variation of measured maximum stress range and fatigue assessments

Regarding the welding joints categorized into C class and D class such as longitudinal welds joining flanges and webs, it should be considered that there is ample allowance to be taken, and therefore it is justified to think that fatigue damage will hardly occur after this. However, the degrees of allowance of welding joints categorized into F class such as ends of

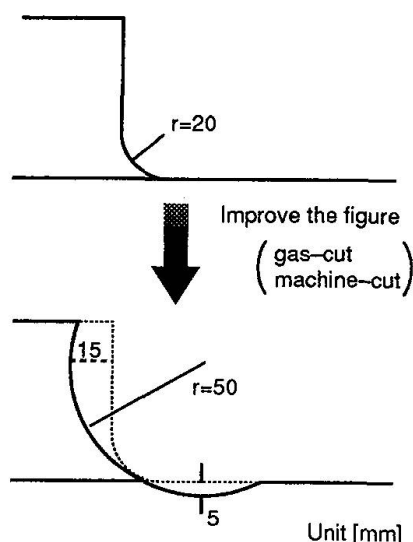


Fig.16 Improving work of flange gusset detail

gussets attached to flanges or fillet welds of sleeper pads attached to flanges are slightly small. This shows the possibility of occurrence of fatigue damage. Hence, these details should be placed under watchful inspections, and remedial measures regarding fatigue strength should be worked out. For example, remedial measures of ends of gussets attached to flanges have been studied. One of conceivable methods is to increase the radius of the fillet at the end of gusset (Fig.15) [9]. Fatigue tests have been carried out and it has been made clear that fatigue strength will be upgraded from F class to C class. Regarding the sleeper pads, this detail and remedial measures are still under study.

5. Concluding Remarks

The service environment of a bridge, such as loading, often differs widely from what had been assumed at the time of designing.

To evaluate the degree of soundness of bridges, preventive works against fatigue damage should be carried out mainly by clarification of fatigue strength of used details and by measurements of actual bridges.

Considering some cases of measurements, the fatigue damage will hardly occur in the details categorized into C class and D class such as longitudinal welds joining flanges and webs hereafter. However the details categorized into F class such as ends of gussets attached to flanges or fillet welds of sleeper pads have the possibility of suffering fatigue damage.

Such preventive programs, including appropriate retrofitting works, have been taken from the early stage of fatigue damage in steel bridges. As a consequence, we are maintaining the tracks in good condition without any serious accidents. However, there is a growing demand for increasing the train speed or transportation capacity. This will probably add more and more to the burden on the structures, therefore researches for upgrading the structural details efficiently and reliable maintenance are becoming more and more important.

References

- 1 NOZAWA, T., et-al ; Present Situation and Problems of the Shinkansen Bridges, Railway Civil Engineering 19-3, 1977.3 (in Japanese).
- 2 Subcommittee for Investigation of Fatigue Damage of Steel Structures, Committee for Structures ; Survey of Fatigue Damages in Steel Bridges, Proceeding of JSCE, No.368/I -5, 1986.4 (in Japanese).
- 3 ISOURA, K. ; Maintenance Program of Shinkansen Structures, IABSE SYMPOSIUM LISBON, 1989.
- 4 SAKAMOTO, K., et-al ; Vibration Fatigue of Steel Bridges on the Bullet Train System, IABSE WORKSHOP LAUSANNE, 157-166, 1990.
- 5 SAKAI, N., et-al ; Consideration of Damage Occurring End Corner of Girder Reducing Section, Proceeding of the 49th Annual Conference of JSCE, I -252, 1994, (in Japanese).
- 6 SAKAGAMI, A., et-al ; Study on the Cause of Fatigue Crack Occurring Sole Plate of Railway Bridge, Proceeding of the 48th Annual Conference of JSCE, I -223, 1993 (in Japanese).
- 7 KAJI, H., et-al ; Stress Measurements of Steel Bridges in Tokaido Shinkansen, Proceeding of the 50th Annual Conference of JSCE, I -394, 1995 (in Japanese).
- 8 MIKI, C. ; Maintenance and Life Extension Works of Steel Bridges in Japan, IABSE SYMPOSIUM, 1995.
- 9 MIKI, C., et-al ; Improving Work of Flange Gusset Detail, Proceeding of the 50th Annual Conference of JSCE, I -388, 1995 (in Japanese).

Proposal of Fatigue Life Evaluation Method for Steel Structural Details under Variable-Amplitude Stresses

Takeshi MORI

Professor
Hosei University
Tokyo, Japan

Takeshi Mori, born in 1955, graduated in civil engineering from Tokyo Metropolitan University in 1978, and received his doctor degree from Tokyo Institute of Technology in 1987.



Summary

Fatigue crack propagation analyses for typical steel structural details are performed under various types of variable-amplitude stresses which can approximately express the stress spectrum in various steel structures. On the basis of the analytical results, the relationship between threshold stress range to give the fatigue damage and the degree of fatigue damage is verified. By using this relationship, a new method is proposed to predict the fatigue life under variable-amplitude stresses.

1. Introduction

Fatigue strength or life of the structural details, which is essential in fatigue assessments for the steel structures subjected to repeated action of loads, is usually obtained from fatigue tests under constant-amplitude stresses. However, stresses occurred on the structural details are rarely constant-amplitude but are usually variable-amplitude. This is so, because the load applied to the actual structure is not fixed and their location is also not definite. The fatigue life under such variable-amplitude stresses is generally obtained from the following processes.

- (1) The stress range histogram is calculated by applying a stress counting method such as the rain-flow method to the stress variations.
- (2) To the stress range histogram and the relationship between stress range and fatigue life ($\Delta\sigma$ - N relationship) under constant-amplitude stresses, a linear cumulative damage law is applied, then the fatigue life is obtained.

As the liner cumulative damage law, some methods have been proposed such as Miner's rule, modified Miner's rule, Haibach's procedure and so on, and they are employed in some fatigue design guidelines.

In the cumulative damage law, the fatigue life is basically calculated on the basis of the following equation :

$$D = \sum D_i = \sum (n_i / N_i) = 1 \quad (1)$$

in which, n_i is the number of repetitions of $\Delta\sigma_i$ which composes the stress range histogram, N_i is the fatigue life when $\Delta\sigma_i$ are repeatedly applied to the objective detail, as shown in Figure 1. D is the cumulative damage and D_i is the fatigue damage due to $\Delta\sigma_i$. In Miner's rule, N_i is directly computed from the relationship between stress range and a fatigue life obtained from constant-amplitude stress tests, that is, N_i is infinite when $\Delta\sigma_i$ is less than the fatigue limit. However, once the fatigue cracks are initiated under the variable-amplitude stresses, a lower stress component below the fatigue limit becomes effective in causing fatigue damage. The Miner's rule therefore results in giving unsafe estimation. In order to improve this problem, the modified Miner's rule and Haibach's procedure were proposed. In the modified Miner's rule, the N_i according to the



$\Delta\sigma_i$ below the fatigue limit is computed from a straight line extended from the relationship above the fatigue limit, as shown in Figure 1. In this case, it is known that an evaluation becomes too conservative. For that reason, it was proposed that a cut-off limit of stress range was set at below the fatigue limit. Hereafter, this method will be called the modified Miner's rule with the cut-off limit. This method has been employed in "Fatigue Design Recommendations for Steel Structures" by the Japanese Society of Steel Construction (JSSC Recommendations) [1], in which the cut-off limit is set at 46% of the fatigue limits.

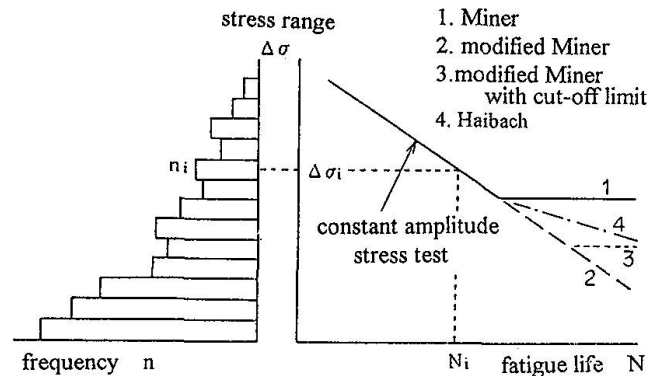


Fig. 1 Linear cumulative damage law

In Haibach's procedure, a slope of $\Delta\sigma$ - N relationship below the fatigue limit is more gentle than that above the fatigue limit, as shown in Figure 1. This slope is $-1/(2m-1)$, where $-1/m$ is the slope in a region of stress range being larger than the fatigue limit. This was derived from the following two assumptions. The first was that the threshold stress range ($\Delta\sigma_w$) providing fatigue damage decreases as the cumulative damage (D) increases as shown in Equation (2).

$$\Delta\sigma_w = \Delta\sigma_{w0} (1 - D)^{1/(m-1)} \quad (\Delta\sigma_{w0} : \text{fatigue limit}) \quad (2)$$

Secondly, the cumulative damage (D) is proportional to the cyclic number of every stress range. Reppermund [2] suggested that the later assumption is invalid, and proposed the new method using only the former assumption. Iida and Koh [3] was discussing the value of exponent in Equation (2) on the basis of the fatigue test results on notched specimens of plain steel.

In this study, the $\Delta\sigma_w$ - D relationship for typical structural details will be discussed on the basis of fatigue crack propagation analyses under various types of variable-amplitude stresses. A proper parameter for representing the relationship between $\Delta\sigma_w$ and D which can be applied to various structural details will be verified, then a new method will be proposed for predicting the fatigue life under variable-amplitude stresses. Estimation by the proposed method will be compared with estimation by previous methods through the results of the fatigue crack propagation analyses and experimental results by Melhem and Klippstein [4].

2. Fatigue crack propagation analysis

2.1 Analytical models

Objective models consist of three kinds. In the first models, a main plate thickness of a cruciform fillet welded joint shown in Figure 2(a) is varied from 9 to 75mm as indicated in Table 1. An attachment plate thickness is the same as that of the main plate. The width of the joint is three times as large as the plate thickness and weld size is a half of the plate thickness. Weld toe radius and flank angle are assumed to be 0.5mm and 135 degrees. An initial crack is a surface one of semi-elliptical form whose depth is 0.1mm and width is 0.4mm. Its position is assumed to be the center of the plate width. The critical crack depth is supposed to be 80% of the main plate thickness.

In the second models, the weld toe flank angle of the cruciform fillet welded joints shown in Figure 2(a) is varied from 100 to 150 degrees. The thicknesses of both the main and attachment plate are 16mm. The width of the main plate is 110mm, and the weld size is 6mm. The initial and final cracks are the same as those of the first models.

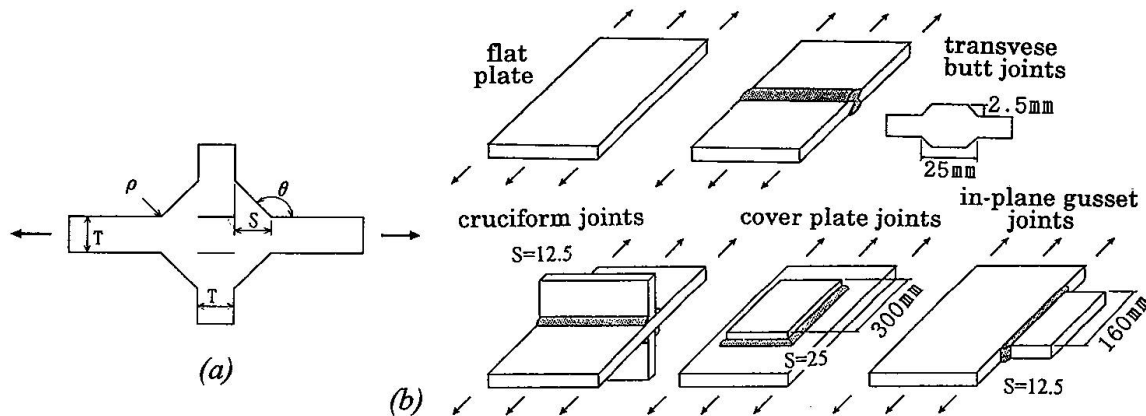


Fig. 2 Analytical models

In the last models, a flat plate, a transverse butt welded joint, a cruciform fillet welded joint, a cover plate welded joint and an in-plane gusset welded joint are taken up. In every joint, its plate thickness is 25mm and its width is 320mm. The flank angle and radius of a weld toe is set at 135 degrees and 0.5mm. The weld size is 12.5mm in the cruciform joint, 20mm in the cover plate joint and 12.5mm in the in-plane gusset joint. For the in-plane gusset joint, the surface initial crack of semi-elliptical form whose depth is 0.1mm and width is 0.4mm is set at the center of the thickness along the weld toe. For other joints, the same initial crack is placed at the center of the width. The critical size of the crack is 80% of the thickness for the cruciform joint and 80% of the width for the other joints.

2.2 Stress range histogram

The fatigue crack propagation analysis will be performed under various stress range histograms which is expressed by the Weibul distribution used in Norwegian standard for mobile offshore structures [5] and is formulated as follows.

$$Q(\Delta\sigma/\Delta\sigma_{\max}) = \exp[-(\Delta\sigma/\Delta\sigma_{\max})^h \ln(N_0)] \quad (3)$$

$Q(\Delta\sigma/\Delta\sigma_{\max})$: cumulative distributed function
 h : parameter for expressing the shape of the distribution
 N_0 : total number of stress cycles
 $\Delta\sigma_{\max}$: maximum stress range

The parameters in this distribution are assumed that h is 0.5, 0.7, 1.0, 1.5, 2.0 and N_0 is 10^4 , 2×10^4 , 5×10^4 , 10^5 , 2×10^5 , 5×10^5 , 10^6 , 10^8 . That is, 40 types of stress range histograms are employed.

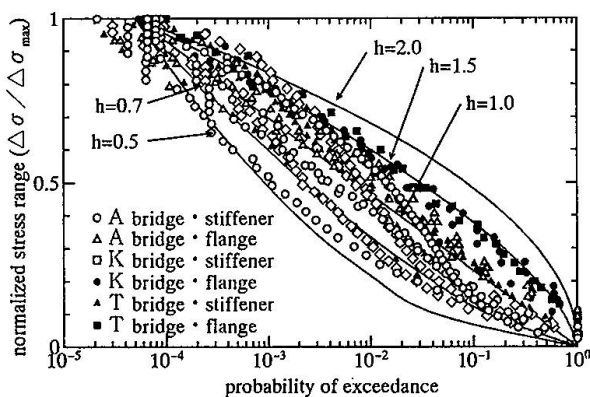


Fig. 3 Cumulative stress range histograms measured in highway bridges

Figure 3 shows the cumulative stress range histograms which were measured on the flange and the stiffener in the actual steel bridges for 24 hours by the Japanese Ministry of Construction [6]. These histograms almost sit between the Weibul distributions of $h=0.5$ and 2.0. In this figure, 23 histograms are presented and N_0 -values in the 23 histograms range from 8,410 to 80,330. The solid lines are shown for the condition that N_0 is equal to 20,000.



2.3 Analytical procedure

The flow of the fatigue crack propagation analysis used here is shown in Figure 4.

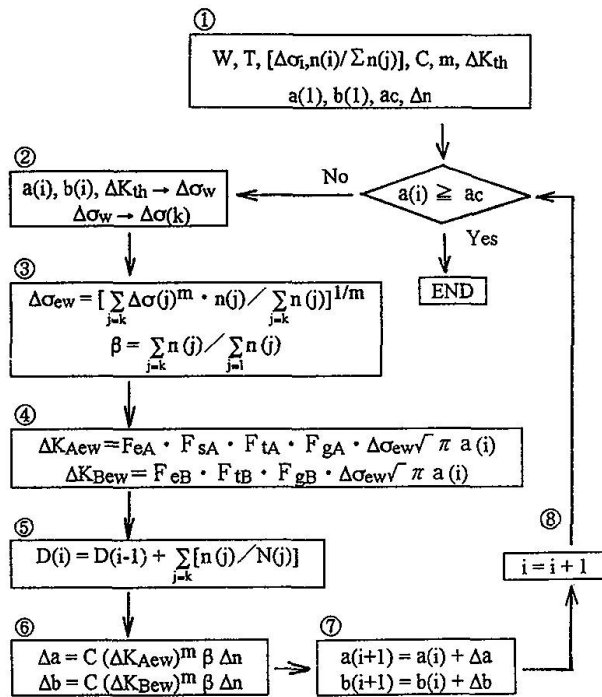


Fig. 4 Process of fatigue crack propagation analysis

- ① The joint sizes (W, T), the initial crack size [a(1), b(1)], the critical crack size (a_c), the material constants for the fatigue crack propagation rate expression (C, m, ΔK_{th}) and the relative stress range histogram [Δσ(j), n(j)/Σn(j)] are inputted.
- ② Threshold stress range (Δσ_w) for a given crack is calculated on the basis of the threshold stress intensity factor range (ΔK_{th}).
- ③ Equivalent stress range (Δσ_{ew}) for the stress components above Δσ_w is calculated. A ratio (β) of frequency of the stress ranges above Δσ_w to that of all the stress ranges is also calculated.
- ④ Equivalent stress intensity factor ranges according to the Δσ_{ew} and the given crack (ΔK_{Aew}, ΔK_{Bew}) are calculated.
- ⑤ The cumulative damage (D) is calculated.
- ⑥ The fatigue crack increments (Δa, Δb) are calculated by using the fatigue crack propagation rate expression.
- ⑦ The crack after extension is defined.
- ⑧ Above processes from ② to ⑦ are repeated until the crack is getting large and reaches the final size.

The fatigue crack propagation rate da/dN is expressed as a function of stress intensity factor range (ΔK) by the following equation.

$$\begin{aligned}
 da/dN &= 5.4 \times 10^{-12} (\Delta K)^3 & [\Delta K > \Delta K_{th}] \\
 da/dN &= 0 & [\Delta K \leq \Delta K_{th}]
 \end{aligned} \tag{4}$$

da/dN : m/cycle,
 ΔK : MPa√m,
 ΔK_{th} = 2MPa√m

Equation (4) has been derived from the statistic analysis using many fatigue crack propagation test results on plain steel and welded steel specimen [7]. The value of the threshold stress intensity factor range (ΔK_{th}) was obtained from the test results on the welded specimens in which the fatigue cracks propagated in high tensile residual stress field [8].

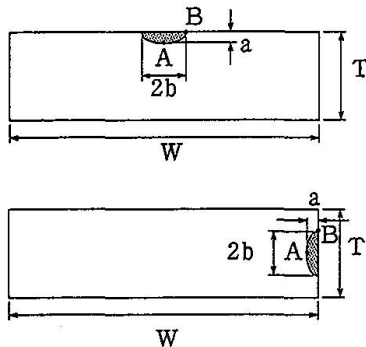


Fig. 5 Definition of a fatigue crack

The stress intensity factor ranges at the deepest point (point A in Figure 5) and the wedge (point B in Figure 5) of the crack are calculated by the following equations :

$$\begin{aligned}
 \Delta K_A &= F_{eA} \cdot F_{sA} \cdot F_{tA} \cdot F_{gA} \cdot \Delta \sigma \sqrt{\pi a} \\
 \Delta K_B &= F_{eB} \cdot F_{sB} \cdot F_{tB} \cdot F_{gB} \cdot \Delta \sigma \sqrt{\pi a}
 \end{aligned} \tag{5}$$

- F_{eA}, F_{eB} : correction factor for crack shape
 F_{sA} : correction factor for surface crack
 F_{tA}, F_{tB} : correction factor for finite thickness and width of plate
 F_{gA}, F_{gB} : correction factor for stress gradient

These correction factors could be calculated using the approach given in [9].

The equivalent stress range for the stress range components above the threshold stress range ($\Delta\sigma_{ew}$) can be obtained from the following equation.

$$\Delta\sigma_{ew} = (\sum \Delta\sigma_i^3 \cdot n_i / \sum n_i)^{1/3} \quad (6)$$

In which, n_i according to $\Delta\sigma_i$ below $\Delta\sigma_w$ is equal to 0.

3. Relationship between threshold stress range and cumulative damage

3.1 Influence of the form of stress range histogram

The relationships between the threshold stress range ($\Delta\sigma_w$) and the cumulative damage (D) are shown in Figure 6(a) for the transverse butt joints and in Figure 6(b) for the cover plate joints, which were obtained from the crack propagation analyses. The ordinates in these figures are the threshold stress range normalized by the fatigue limit ($\Delta\sigma_w/\Delta\sigma_{w0}$). In these figures, analytical results for ten forms of the stress range histograms are indicated, and $\Delta\sigma_w/\Delta\sigma_{w0}$ - D relationships are not dependent on the form in both joints. This fact was common in other forms of the stress range histograms and other type of joints.

The results shown in Figures 6(a) and (b) were obtained when the maximum stress range ($\Delta\sigma_{max}$) was set at four times as large as $\Delta\sigma_{w0}$. However, $\Delta\sigma_w/\Delta\sigma_{w0}$ - D relationships were not also influenced by the value of $\Delta\sigma_{max}$.

mark	weibul parameters	mark	weibul parameters
○	$h=0.5, No=5 \times 10^4$	●	$h=0.5, No=5 \times 10^5$
△	$h=0.7, No=10^4$	▲	$h=0.7, No=10^8$
□	$h=1.0, No=10^8$	■	$h=1.0, No=2 \times 10^5$
▽	$h=1.5, No=2 \times 10^4$	▼	$h=1.5, No=10^5$
◇	$h=2.0 \times 10^8$	◆	$h=2.0, No=5 \times 10^4$

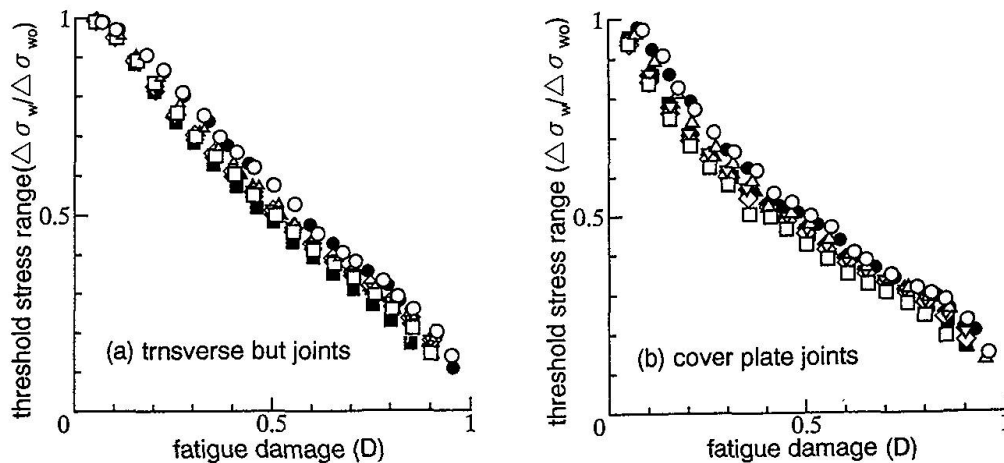


Fig. 6 Influence of stress range histogram on $\Delta\sigma_w$ - D relationship

3.2 Influence of plate thickness

For the models in which the plate thickness of the cruciform fillet welded joints is varied from 9 to 75mm, the stress concentration factor obtained from the finite element analyses and fatigue strength at two million stress cycles calculated by the fatigue crack propagation analyses under constant-amplitude stresses are also shown in Table 1. In the finite element analysis, a plane strain element was used, and the minimum element size was set at 0.025mm. These conditions are common to other types of models. As the plate thickness is increasing, the stress concentration is also becomes higher and the fatigue strength becomes lower.



Figure 7 shows the $\Delta\sigma_w/\Delta\sigma_{w0}$ -D relationships which were obtained from the crack propagation analyses under variable-amplitude stresses. The form of $\Delta\sigma_w/\Delta\sigma_{w0}$ -D relationship becomes concave as the plate is getting thicker, that is, the fatigue strength is decreasing.

model	thick- ness	stress concentration factor	fatigue strength at 2million stress cycles	exponent C
AT	9mm	2.48	178.0MPa	1.23
BT	16mm	2.82	105.0MPa	1.15
CT	25mm	3.25	95.7MPa	1.06
DT	35mm	3.61	89.3MPa	1.00
ET	45mm	3.98	84.8MPa	0.94
FT	75mm	4.61	75.9MPa	0.87

Table 1 Models of varying thickness

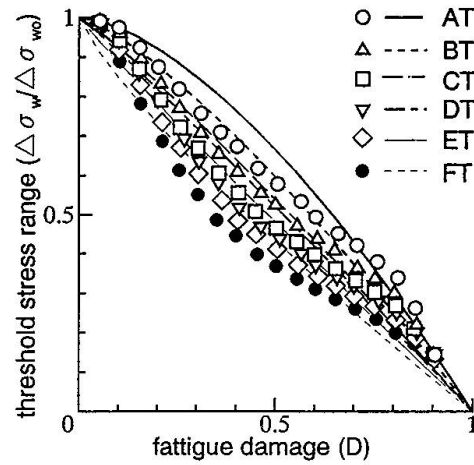


Fig. 7 Influence of thickness on $\Delta\sigma_w$ -D relationship

3.3 Influence of flank angle

The stress concentration factor and the fatigue strength at two million stress cycles obtained for the models of varying a flank angle of the weld toe are indicated in Table 2. As the flank angle is getting smaller, the stress concentration factor becomes higher and the fatigue strength becomes lower. It can be seen from Figure 8 that as the fatigue strength becomes lower, the form of the $\Delta\sigma_w/\Delta\sigma_{w0}$ -D relationship becomes more concave. This fact is the same as that in the models of varying thickness.

model	flank angle	stress concentration factor	fatigue strength at 2 million stress cycles	exponent C
F150	150B	2.42	96.6MPa	1.24
F135	135B	2.76	90.3MPa	1.17
F120	120B	3.17	84.7MPa	1.11
F100	100B	3.26	81.4MPa	1.08

Table 2 Models of varying weld toe geometry

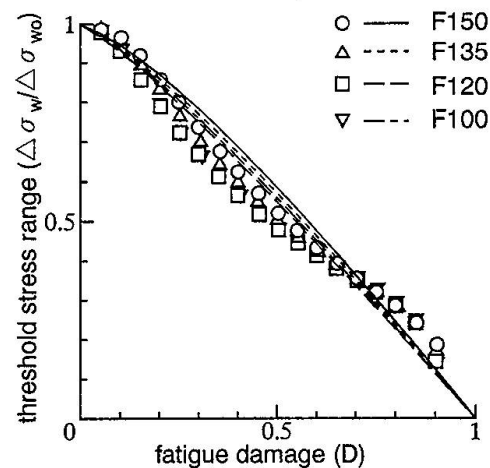


Fig. 8 Influence of flank angle on $\Delta\sigma_w$ -D relationship

3.4 Influence of joint type

The stress concentration factor and the fatigue strength at two million stress cycles obtained for each joint indicated in Figure 2(b) are shown in Table 3, and the $\Delta\sigma_w/\Delta\sigma_{w0}$ -D relationships for these joints are illustrated in Figure 9. In the same way as the two types of models mentioned above, while the fatigue strength at two million stress cycles becomes lower, the form of the $\Delta\sigma_w/\Delta\sigma_{w0}$ -D relationship becomes more concave.

model	stress concentration factor	fatigue strength at 2 million stress cycles	exponent C
flat plate	1.00	178.0MPa	2.06
transverse butt joint	2.32	116.9MPa	1.45
cruciform joint	3.02	86.0MPa	1.12
cover plate joints	3.86	76.3MPa	1.02
in-plane gusset joints	10.95	47.6MPa	0.68

Table 3 Models of varying joint type

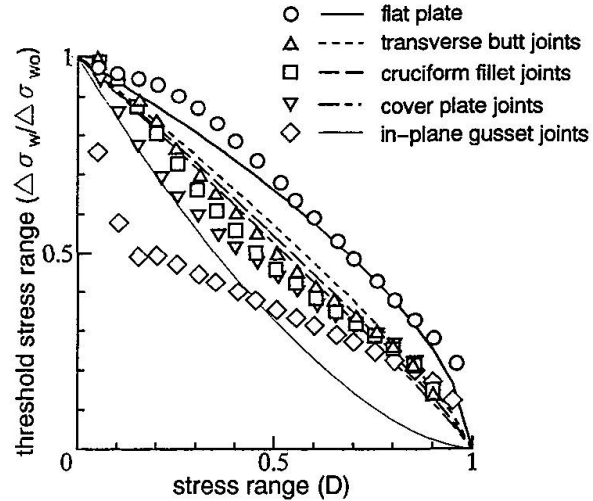


Fig. 9 Influence of joint type on $\Delta\sigma_w$ -D relationship

3.5 Expression for the $\Delta\sigma_w/\Delta\sigma_{w0}$ -D relationship

The $\Delta\sigma_w$ -D relationships shown in Figures 7, 8 and 9 will be expressed by Equation (7) :

$$\Delta\sigma_w = \Delta\sigma_{w0}(1 - D^c) \quad (7)$$

in which, an exponent (c) is a parameter which expresses the form of the $\Delta\sigma_w$ -D relationship. When c is equal to unity, the relationship is linear. The form is concave if c is less than unity and convex if c is larger than unity. The value of c for each model is shown on the right hand column of Tables 1, 2 and 3, which was obtained from the least square method. The relationship obtained by the substitution of the c value into equation (7) is also illustrated in Figs.7 to 9. Only a $\Delta\sigma_w$ -D relationship for one stress range histogram was shown in Figs.7 to 9, but the value of c was obtained by using the data regarding the relationships in all the stress range histograms (40 types) and 5 to 15 values of $\Delta\sigma_{max}$ for each histogram.

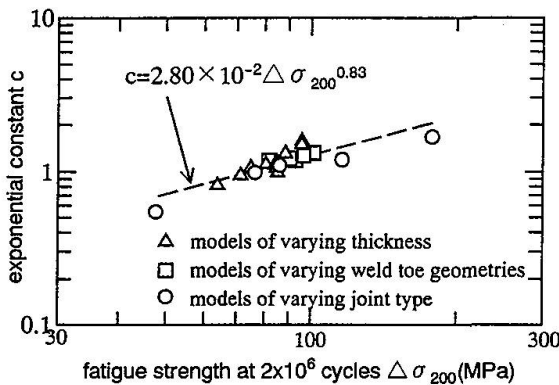


Fig. 10 c - $\Delta\sigma_{200}$ relationship

As mentioned in Sections 3.2 to 3.4, lowering the fatigue strength at two million stress cycles caused the form of the $\Delta\sigma_w$ -D relationship to be concave, that is, it effected the value of c to become smaller. The relationship between the values of c and the fatigue strength at two million stress cycles ($\Delta\sigma_{200}$) is shown in Figure 10. This relationship can be expressed by a straight line in both the logarithmic scales. The following expression indicates the c - $\Delta\sigma_{200}$ relationship calculated by the least square method.

$$C = 2.80 \times 10^{-2} \Delta\sigma_{200}^{0.83} \quad (8)$$

4. Proposal of fatigue life evaluation method

In this study, the following method is proposed for evaluating the fatigue life under variable-amplitude stresses.

- (1) The relationship between stress range ($\Delta\sigma$) and fatigue life (N), the fatigue strength at two million stress cycles ($\Delta\sigma_{200}$) and the fatigue limit ($\Delta\sigma_{w0}$) under constant-amplitude stresses is determined on the basis of the fatigue test results on the objective joints.
- (2) By substitution of $\Delta\sigma_{200}$ into equation (8), the value of the exponent c is determined.



- (3) By substituting $\Delta\sigma_{w200}$ from step (1) and the value of c from step (2) into Equation (7), $\Delta\sigma_w$ - D relationship is determined.
- (4) By using the stress range component ($\Delta\sigma_i$) larger than $\Delta\sigma_w$ obtained from equation (7), its relative frequencies(γ_i) and fatigue life (N_i) according to $\Delta\sigma_i$, the cumulative damage is calculated.

$$D = \sum(\gamma_i \Delta n / N_i) \quad (\text{if } \Delta\sigma_i \text{ is less than } \Delta\sigma_{wo}, N_i = \infty)$$

(Δn is a certain number stress cycles for reducing the number of repeating calculation.)

- (5) Step (4) is repeated until the value of D reaches unity.

5. Comparison with other methods

5.1 Results of fatigue crack propagation analyses

Figures 11(a) and (b) show the relationship between the equivalent stress range ($\Delta\sigma_e$: is calculated by using all the stress range components) and fatigue life for the transverse butt joint and the cover plate joint, in which the relationship is calculated by the fatigue crack propagation analyses, and estimated by the proposed method and previous methods. In both cases, estimated results by each method are almost the same as those by the analyses in a region where stress range is comparably large. On the other hand, in a region where the stress range is small, Miner's rule results in unsafe estimation and the modified Miner's rule give too conservative evaluation. The modified Miner's rule with the cut-off limit slightly result in conservative estimation. Haibach's procedure and Rempermund's procedure produces good estimation for the cover plate joints, but gives a little conservative evaluation for the transverse butt joints. Comparing with those of the previous methods, the estimated fatigue life by the proposed method could express the results of the fatigue crack propagation analyses well in the whole region.

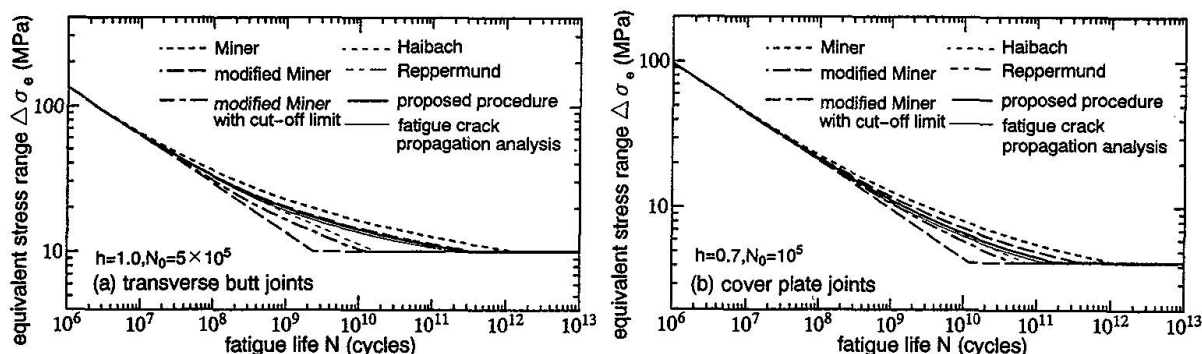


Fig. 11 Relationships between the equivalent stress range and the fatigue life

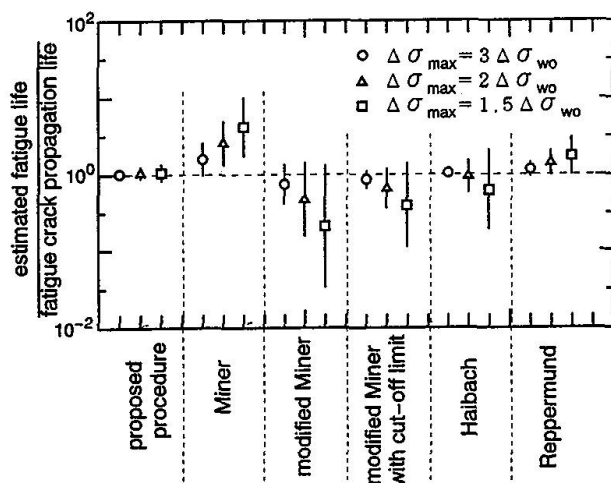


Fig. 12 Comparison of fatigue lives estimated by each method

In order to clarify the differences between the estimated fatigue lives by each method in a region where the stress range is relatively small, the fatigue lives for all the stress range histograms (40 types) and all the models (14 types) are compared for the case that the maximum stress range ($\Delta\sigma_{max}$) is 1.5, 2 or 3 times as large as the fatigue limit ($\Delta\sigma_{wo}$). These results are shown in Figure 12. The ordinate is the fatigue life estimated for each method normalized by that obtained from the fatigue crack propagation analysis. Each mark in the figure shows the average of the normalized fatigue lives and the vertical line indicates the region of the average \pm two standard deviations. The normalized fatigue life by the proposed method is almost unity and its deviation is small compared to that of the previous methods.

5.2 Experimental results by Melhem and Kippstein

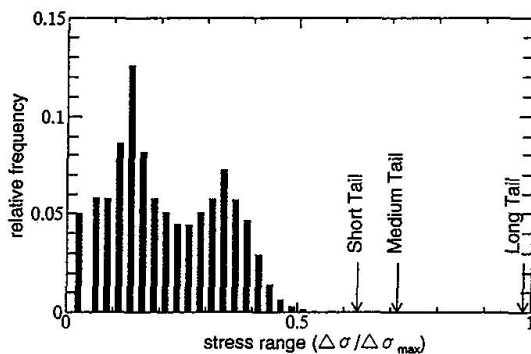


Fig. 13 Stress range histogram used in the tests

Melhem and Kippstein [4] carried out the fatigue tests on the cruciform fillet welded joints (whose thickness is 9.5mm and width is 50.8mm) under constant-amplitude and variable-amplitude stresses. This variable-amplitude stresses simulated the stresses due to the bending moments arising when trucks are passing over the simple supported bridge of 30m span. In this simulation, a distribution of the truck weight was taken into account. The stress range histogram according to the variable-amplitude stresses is shown in Figure 13. This histogram was further divided into three types. Long tail, medium tail and short tail distributions were obtained on the assumption that the truck heavier than 95, 68 and 45 t would not pass, respectively. The materials used for the specimens are A572 steel and A588 steel. The specimens of A572 steel were tested under three kinds of histograms, and those of A588 steel were done under the medium tail distribution only.

Figures 14(a), (b), (c) and (d) show the fatigue test results and the estimated relationships between equivalent stress range ($\Delta\sigma_e$, including all the stress range components) and fatigue life (N) by the proposed method and previous methods. In every series of tests, $\Delta\sigma_e$ - N relationships were obtained up to the region of fatigue lives of eight figures. Until this region, the estimated results by each method are not so different from each other. Observing them in detail, the estimation by Miner's rule, which is considered to give an unsafe estimation, is the closest to the fatigue test results indicated in Figures 14 (a) and (b), and the proposed method is followed. For the test results shown in Figures 14(c) and (d), the proposed method gives the nearest estimation.

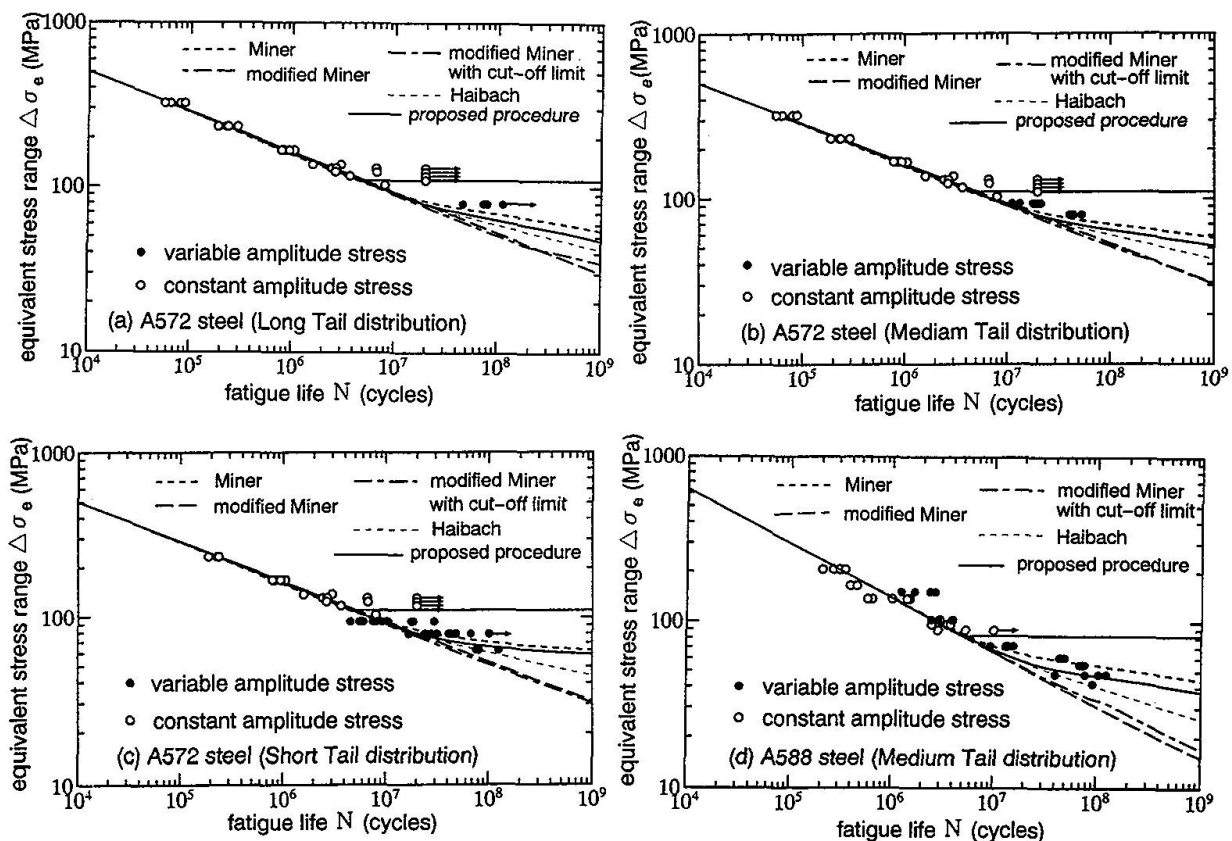


Fig. 14 Comparison of estimated results with the test results



6. Conclusions

- (1) The relationship between the threshold stress range and the degree of fatigue damage is significantly influenced by stress distributions in the details. This relationship therefore depends on the type of details, the plate thickness and weld toe geometry.
- (2) The relationship for a detail is considerably related to its fatigue strength under constant-amplitude stresses, and can be expressed by the following equation :

$$\Delta\sigma_w = \Delta\sigma_{w0} (1 - D^c)$$

where $c = 2.80 \times 10^{-2} \Delta\sigma_{200}^{0.83}$

$\Delta\sigma_w$: threshold stress range

$\Delta\sigma_{w0}$: fatigue limit under constant-amplitude stress

D : degree of fatigue damage based on a linear cumulative damage concept

$\Delta\sigma_{200}$: fatigue strength at 2 million stress cycles.

- (3) The fatigue life evaluation method is proposed by combining the above equation with the linear cumulative damage concept. The validity of the proposed method has been confirmed through the comparisons of fatigue lives estimated by the proposed method to analytical results by crack propagation analysis and to experimental results by Melhem et al.

References

1. JAPANESE SOCIETY OF STEEL CONSTRUCTION. Fatigue Design Recommendations for Steel Structures. JSSC Report No.32, 1995.
2. REPPERMUND, K. Ein Konzept zur Berechnung der Zuverlassigkeit bei Ermudungsbeanspruchung, Stahlbau, 4/1986, pp.104-112, 1986.
3. IIDA, K. ; KOH, H. Cumulative Fatigue Damage under p-distribution Loads (2nd report), Proc. of The Soc. of Naval Architects of Japan, No.152, pp.372-380, 1982 (in Japanese).
4. MELHEM, H.G. and KLIPPSTEIN, K.H. A study on Variable-amplitude Load Fatigue (work-in-Progress), Research Report No.ST-6, Department of Civil Engineering, University of Pittsburgh, 1990.
5. DET NORSKE VERITAS. Fatigue Strength Analysis for Mobile Offshore Units, Classification Note No.30.2, 1984.
6. CIVIL ENGINEERING RESEARCH INSTITUTE (Japanese Ministry of Construction). A Research on the Techniques about Estimation and Improvement of the Endurance of Existing Bridges, Report of Civil Engineering Research Institute, No.2420, 1990 (in Japanese).
7. OKUMURA, T., NISHIMURA, T., MIKI, C. AND HASEGAWA, K. : Fatigue Crack Growth in Structural Steel, Proceedings of Japanese Society of Civil Engineers, No.322, pp.175-178, 1982.
8. MIKI, C. ; MORI, T. ; TAJIMA, J. Effect of Stress Ratio and Tensile Residual Stress on near Threshold Fatigue Crack Growth, Proceedings of the Japanese Society of Civil Engineers, No.386, pp.383-392, 1986.
9. MIKI, C. Fatigue Model (Japanese Society of Steel Construction. Reliability Estimation for Civil Structures, Section 5.2), JSSC Report, No.13, pp.89-109, 1989 (in Japanese).

Material Identification and Verification Method for the Residual Safety of Old Steel Bridges

G. STÖTZEL Dipl.-Ing. RWTH Aachen, Germany	G. SEDLACEK Prof. Dr.-Ing. RWTH Aachen, Germany	P. LANGENBERG Dr.-Ing. RWTH Aachen, Germany	W. DAHL Prof. Dr. RWTH Aachen, Germany
--	---	---	--

Gero Stötzel, born in 1964, received his degree in civil engineering at the RWTH Aachen. Since 1991 he has been working at the Institute of Steel Construction in the field of structural safety and fracture mechanics.

Gerhard Sedlacek, born in 1939, received his degree in civil engineering at the TU Berlin. For eight years he worked in the steel industry. Since 1976 he has been Professor of Steel Structures at RWTH Aachen.

Peter Langenberg, born in 1962, studied metallurgy and material science and obtained his degree at the RWTH Aachen in 1995. He is working at the Institute of Ferrous Metallurgy in the field of structural safety and fracture mechanics.

Winfried Dahl, born in 1928, received his degree in physics at Georgia-Augusta University in Göttingen, FRG. From 1969 until 1993 he was the head of the Institute of Ferrous Metallurgy at the RWTH Aachen. He is still working in the field of metal engineering and fracture mechanics at the Institute of Ferrous Metallurgy.

Summary

This paper presents a method to determine the residual safety and service life of old steel bridges on the basis of a fracture mechanics based toughness verification. The reliability of this method has been improved on the basis of statistical evaluations of material properties of old steel bridges that have been used to derive safety elements for the model uncertainty according Eurocode 3, Part 1.1 - Annex Z [10].

1. Introduction

A great part of existing steel bridges for roads and rails are riveted structures that were built in the last century. Many of these old bridges have undergone several phases of repair or strengthening after damages in the world wars or due to changes of service requirements. For these bridges the question of the actual safety for modern traffic loads and the remaining service life is put forward.

A procedure to determine the residual safety and service life of old steel bridges on the basis of fracture mechanics based toughness verifications has been developed in close co-operation between the Institute of Ferrous Metallurgy and the Institute of Steel

Construction of RWTH Aachen. The results may be used for economic decisions for either the further strengthening of an old bridge or the replacement by a new bridge [1], [2], [3], [4], [5]. The method has been applied to many steel bridges in particular in Eastern Germany [6], [7], [8] and also to other structures susceptible to fatigue, e.g. guyed masts, antennae, structural machinery parts etc.

During the last years intensive research works [9] have been carried out to improve the reliability of the method on the basis of statistical evaluations of material properties of old steel bridges and to derive safety elements for the model uncertainty according Eurocode 3, Part 1.1 - Annex Z [10]. This improved method will be presented in the following.



2. The basis of the toughness verification

2.1 Brittleness and ductility

A structural member to be assessed for its residual safety may, due to its prior damages and undetected cracks, react to tension loads by different failure modes which influence the model for calculating the action effects. These failure modes may be best distinguished by the example of a plate in tension with a central crack (Figure 1) that models a member with a hole with cracks on both sides:

- unfavourable failure is exhibited, when fracture occurs before net section yielding with only local yielding at the crack tips. In this case all actual stresses in the net section comprising residual stresses, stress concentrations and stresses due to other restraints have to be taken into account. This failure mode is commonly called "brittle" failure;
- if failure occurs by failure after net section yielding, only the nominal stresses due to external loads in the net section are relevant and notch effects, residual stresses and stresses due to other restraints may be neglected. This mode is called "ductile" failure.

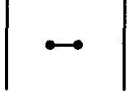
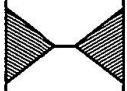
yielding pattern	failure mode	design values
	brittle fracture before net-section yielding	applied stress distribution in the net section + residual stresses + restraints
	ductile fracture after net section yielding	applied nominal stress distribution in the net-section

Fig. 1 Definition of failure modes and the applied design values of stresses dependent on the ductility

The failure mode is mainly influenced by material, temperature, loading rate and shape of the structural member. For old steel bridges both failure modes 1 and 2 are relevant, as the assessment has to be carried out for design situations with low temperatures, where the toughness values are low.

2.2 Determination of vital elements

The toughness-related safety checks are restricted to risk areas with high failure consequences. Therefore, failure scenarios have to be established, where the consequences of failure of different bridge elements for different design situations are investigated (Figure 2). Vital elements are those bridge elements, the failure of which would cause an immediate overall collapse. Vital elements loaded in tension have to be checked in view of toughness-controlled failure unless their cross-sections are sufficiently redundant (Figure 3) so that they do not produce risks. Sufficient redundancy is supposed to be available when crack affected parts of the cross-section may fail without the yield strength being exceeded in the residual cross-sectional parts.

The check shall be based on several loading cases with combinations of self weight, traffic loads including dynamic impact and temperature, which can be based on probabilistic approaches, and with and without residual stresses and restraints depending on the expected failure mode.

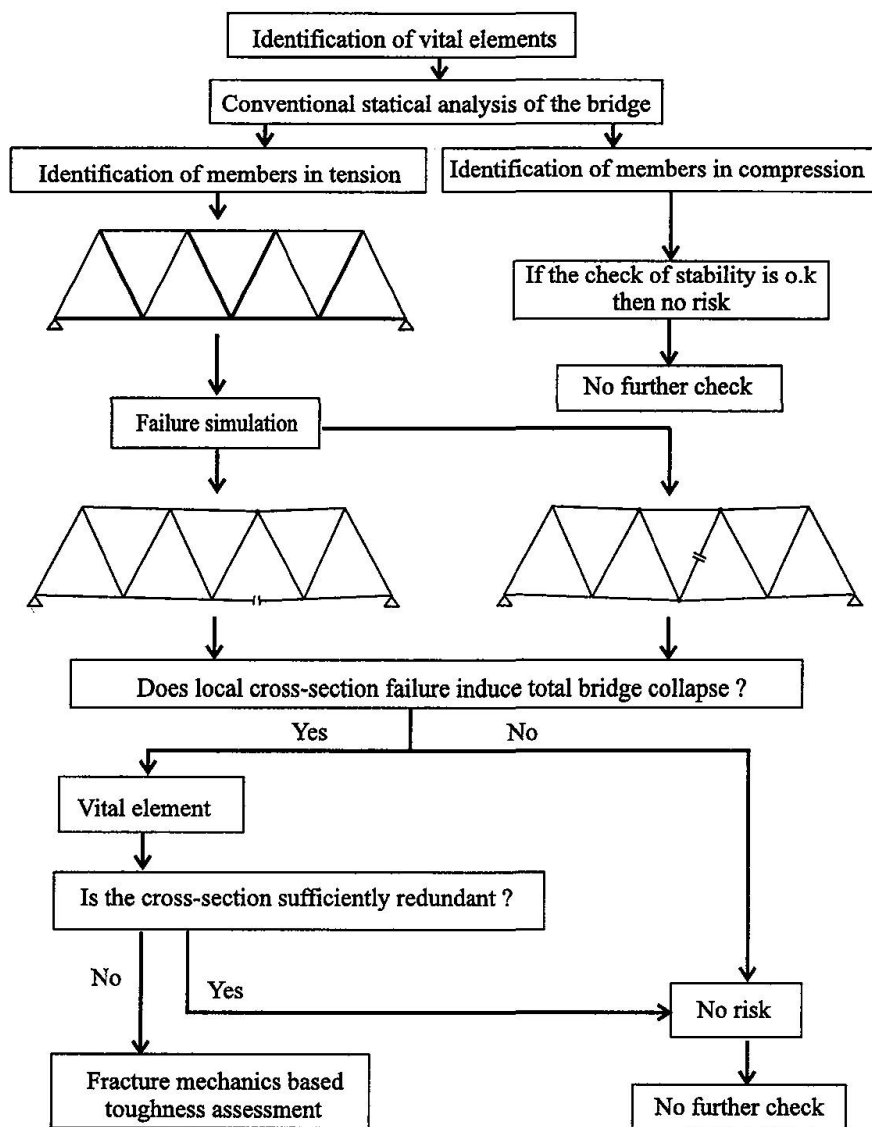


Fig. 2 Procedure for the identification of vital elements

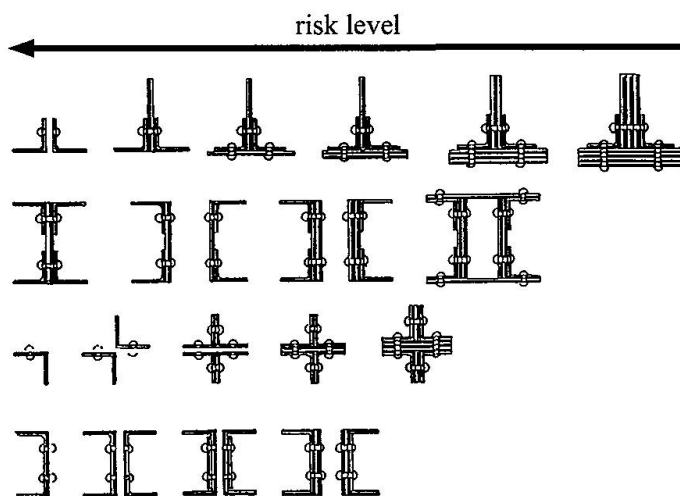


Fig. 3 Typical cross-section of old riveted steel bridges



2.3 Assumption of initial cracks

The toughness assessment requires assumptions on the prior damage of the structure, expressed in terms of initial cracks. From fatigue tests with parts taken from old steel bridges it is known that cracks in old riveted bridges most probably initiate under the rivet heads propagating through the plate thickness and the widths of the outer plates [11]. Hence, it is assumed that on both sides of a rivet hole initial cracks may have formed that have just reached a sufficient size to be detectable. This limit is considered to be 5 mm coming out of the rivet head (Figure 4 a). It has been proved by comparative studies that such a crack configuration may be modelled by a single crack with the initial size $a_0 = D + 2.5$ mm only. In case cracks are assumed to initiate in plates covered by angles (Figure 4 b), the initial crack size is considered such, that a detectable crack size of 5 mm comes out of the flanges of the angle.

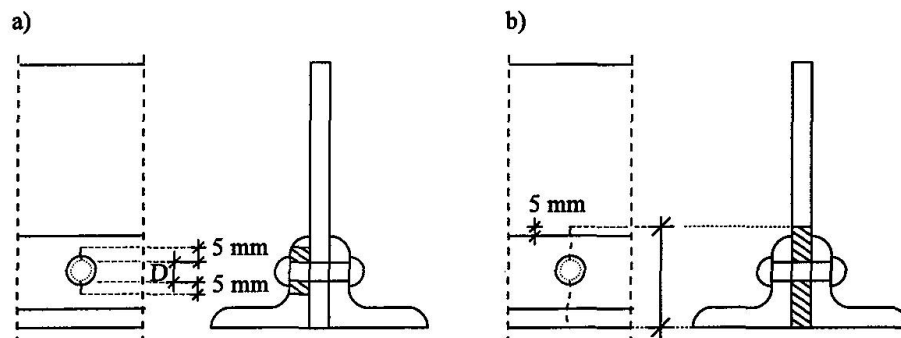


Fig. 4 Assumption for the initial crack size a_0 for a) angles, b) plates covered by angles

2.4 Basic verification principles

For a given loading case, true-stress true-strain curve and crack situation e.g. for the initial crack size a_0 in a vital element, a fracture mechanic action effect in terms of the crack driving energy J_{appl} may be calculated, see 2.5 (Figure 5). The curve $J_{appl} - \sigma_{appl}$ allows to determine whether the applied stresses lead to net section yielding ($J_{appl} > J_{yield}$) or not ($J_{appl} < J_{yield}$).

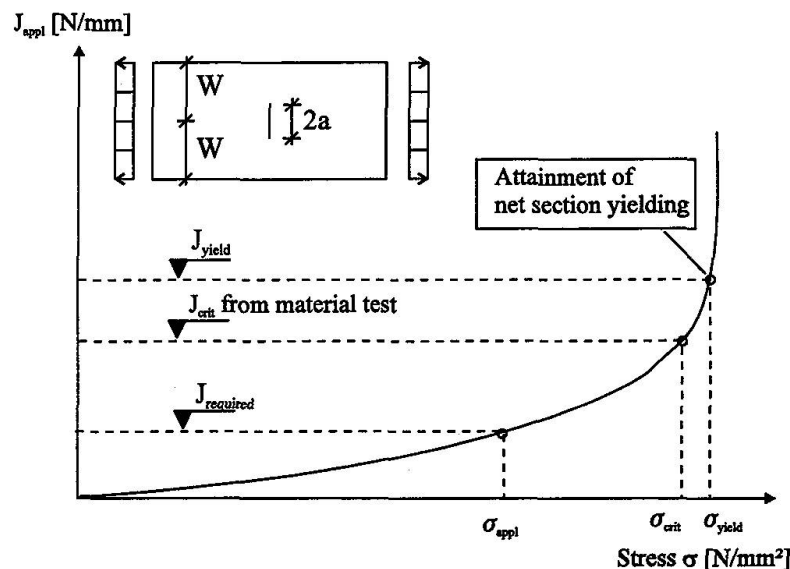


Fig. 5 Typical $J_{appl} - \sigma_{appl}$ diagram for a given plate model with a crack size a

Either from prior knowledge (see 2.6) or from the miniaturised plate samples (Figure 6) 1/2 CT-10 samples the crack extension resistance J_{crit} may be determined for a given temperature. This value may be compared with J_{appl} in the toughness safety verification (see Figure 5):

$$J_{appl} \leq J_{crit} \quad (1)$$

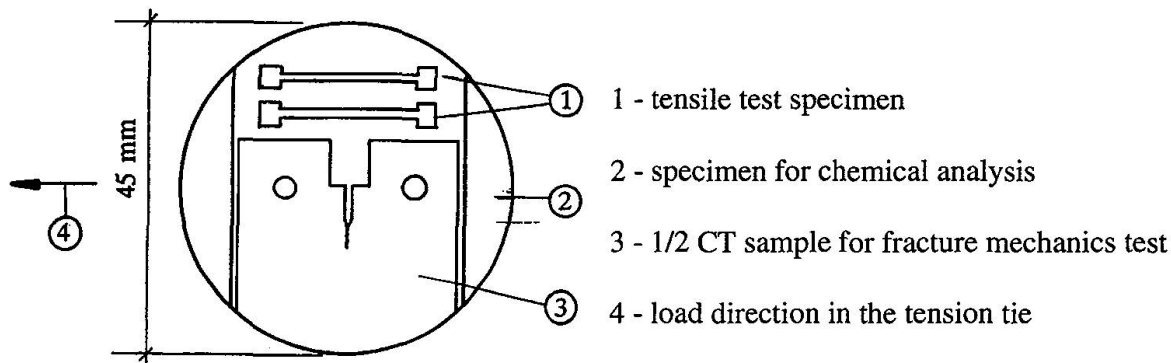


Fig. 6 Miniaturised plate sample

In case J_{appl} has been calculated for an initial crack size a_0 and J_{appl} is smaller than J_{crit} it can be concluded that cracks with detectable sizes are acceptable for the bridge without catastrophic consequences and a collapse without warning will not occur if the bridge has been sufficiently inspected. If this check is not positive, the member has to be strengthened with tough material or to be replaced before the next cold season (loss of toughness at low temperatures).

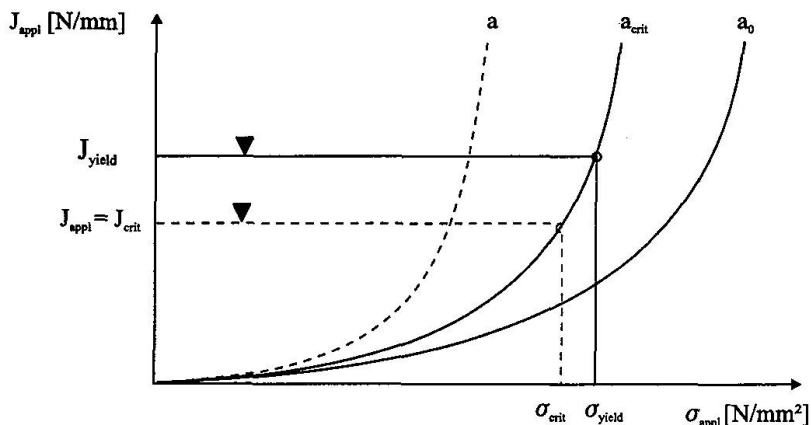


Fig. 7 Determination of a_{crit} by iterative variation of a -values

The critical crack size a_{crit} may be determined by iterative variation of the crack size. It fulfils

$$J_{appl} = J_{crit} \quad (2)$$

(Figure 7) and by definition leads to failure. From the position of J_{yield} in this diagram it can be found out whether failure will occur before or after net section yielding and the consequences for the design values for the action side can hence be taken (Figure 5).

The difference $\Delta a = a_{crit} - a_0$ is a measure for the minimum service time from the detection of cracks until failure. It should at least cover the time interval $t_{insp} + 1.5 \text{ years}$ between two inspections where 1.5 years is an additive safety element. To verify that this minimum service time is sufficient, the crack propagation time t_p is calculated by using information on the magnitude and intensity of the traffic and the Paris equation as the calculation model (Figure 8). If

$$t_{insp} + 1.5 \text{ years} \leq t_p \quad (3)$$

no further actions are necessary. Otherwise either the inspection intervals must be shortened or the member must be strengthened to increase t_p . If the check $t_{insp} + 1.5 \text{ years} \leq t_p$ is positive, the inspections at safe intervals at the critical locations of the vital elements will allow the following conclusions that may be considered as the answers to the questions put above:

As long as no cracks are observed, the structure is sufficiently safe and fit for at least the service period up to the next inspection. This statement can be repeated after each inspection up to the point when first cracks are found. In case they are found there is sufficient time to react by replacing the members or the total bridge.

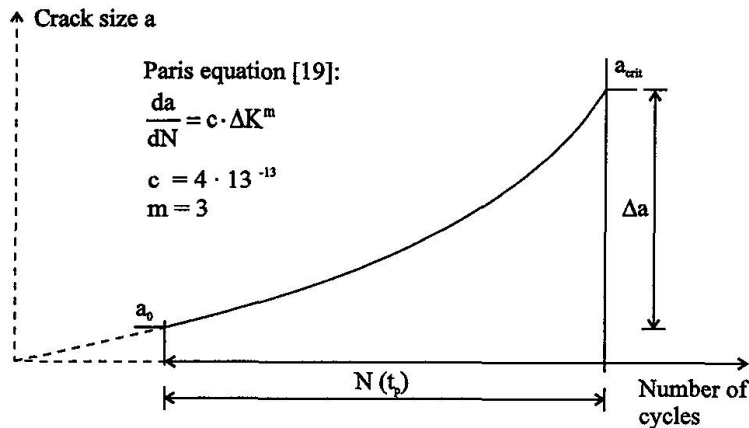


Fig. 8 Principle for the determination of minimum service time $N(t_p)$

2.5 The use of the J-integral

The J-integral as description of the material toughness is defined by [13], [14] (Figure 9). It allows a numerical quantification of the toughness related safety and can be taken from handbooks or calculated by FEM with special grids of collapsed iso-parametric elements (Figure 10). The J_{crit} -values may be determined in experienced laboratories.

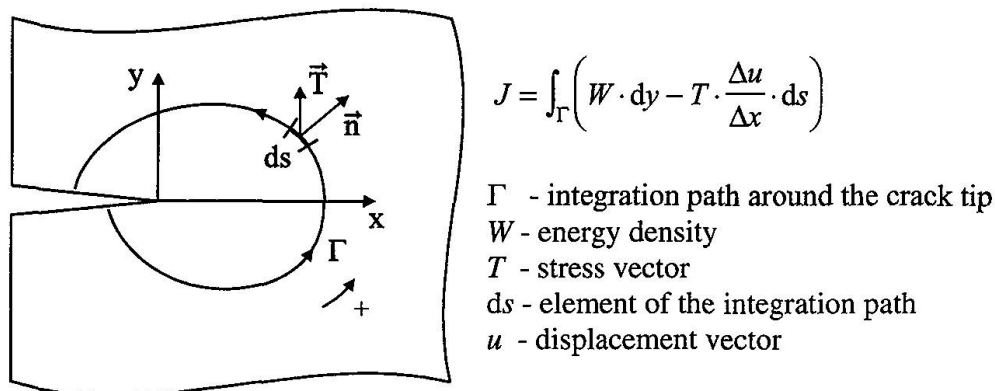


Fig. 9 Definition of the J-Integral

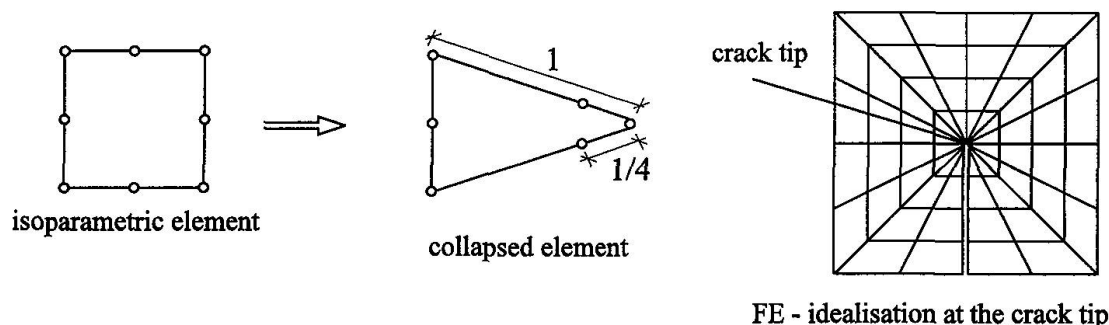


Fig. 10 Finite element and FE-grid for calculating J_{appl}

2.6 Material identification and properties

In old riveted bridges wrought iron as well as puddle iron has been used. Wrought iron has similar properties in chemical composition and microstructure to low strength-low alloy steels of today and is applicable to the fracture mechanics safety assessment. Puddle iron has an totally different microstructure, which can be characterised as laminar type, build up from ferrite and slag. To distinguish specimens taken from riveted bridges after their original production method

by means of chemical and/or metallographical analysis a schema has been developed [15] which is presented in Figure 11.

Based on a statistical evaluation of the chemical and the microstructure properties of 407 specimen from riveted bridges, it was also concluded, that the obtained data for the strength and toughness of wrought iron could be treated as a statistical homogenous population.

The statistical distribution of the material strength has been derived from an amount of 205 tests at 0°C and 283 tests at -30°C. Table 1 shows the results in terms of mean values, standard deviations and fractiles. The Lognormal distribution fitted best for the statistical description of the characteristic strength.

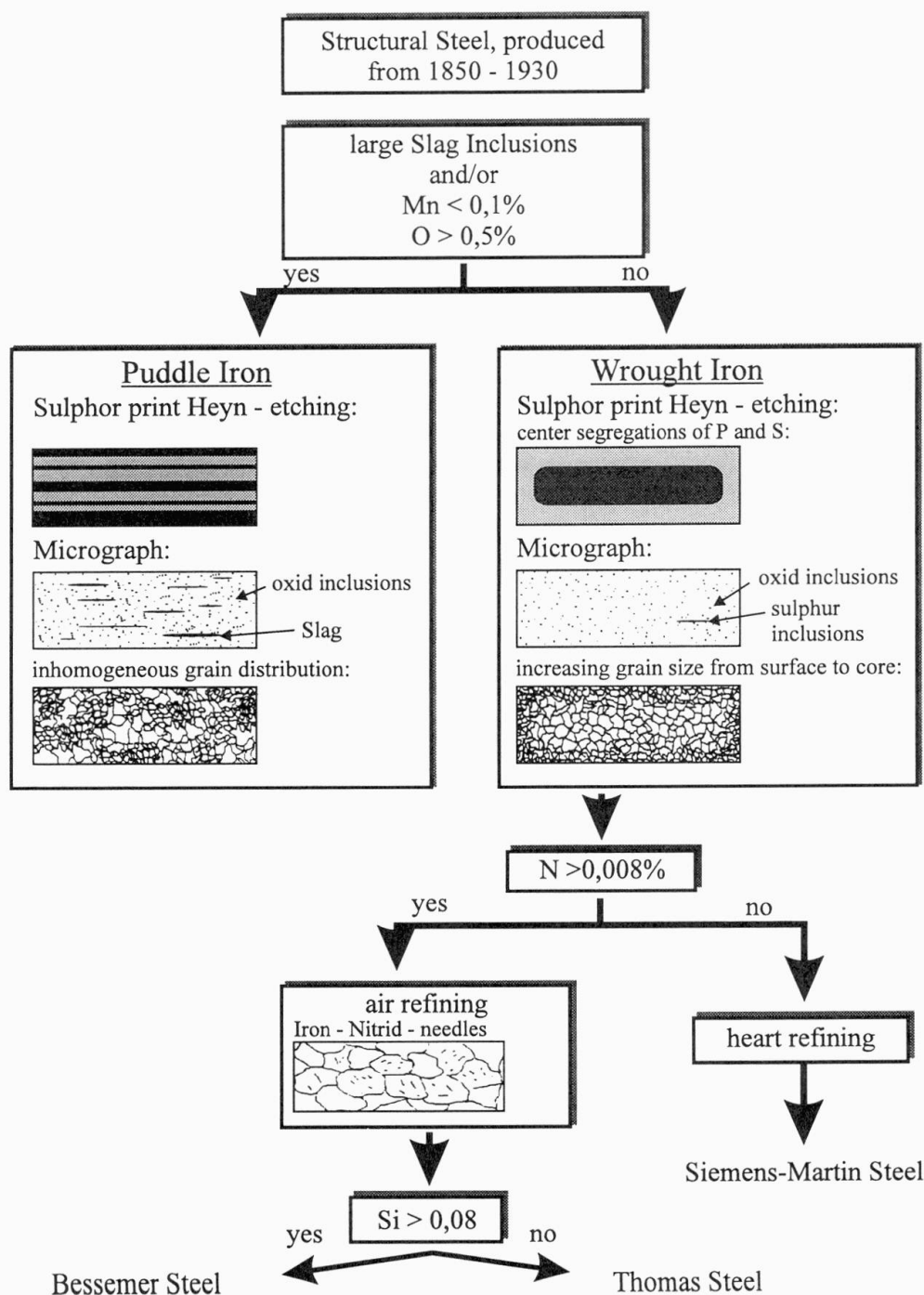


Fig. 11 Identification scheme for old steels



	R_{eL}	R_m	R_{eL}	R_m	A	Z	J_{crit}	J_{crit}
T [°C]	-30	-30	0	0	0	0	-30	0
Typ	Log.	Log.	Log.	Log.	NV	NV	Weib.	Weib.
$x_{0,05}$	257	385	248	374	26	57	17	30
$x_{0,50}$	310	446	293	423	34	66	62	91
$x_{0,95}$	375	516	345	479	41	75		
Log. = Log-normal distributed, NV = normal distributed, Weib. = Weibull distributed (3-parameter), R_{eL} = Yield Strength, R_m = Yield Stress, A = Fracture Elongation, Z = Reduction of Area, J_{crit} = Fracture Toughness acc. [16]								

Table 1 Characteristic values of strength, fracture strain and fracture toughness distributions for wrought iron from 412 tests

If material tests from the bridge shall be avoided, a conservative safety assessment may be carried out with the combination of 5% fractiles for -30 °C:

$$R_{eL} = 257 \text{ N/mm}^2 \text{ and } J_{crit} = 17 \text{ N/mm}$$

3. A new practical verification procedure

3.1 General

The iterative process needed to calculate a_{crit} with the J-integral concept as indicated above is rather time-consuming, expensive and appears to be restricted to fracture-mechanic experts only. Therefore, a more simplified presentation of the method was looked for to make the toughness verification as easy as a conventional strength verification.

3.2 Determination of a_{crit}

This simplified method has been developed in [17] by using three basic plate models with initial crack configurations (Figure 12) which may be considered as representative for any structural detail of riveted steel members. For these three models the values a_{crit} may be easily determined depending on the stress level $d = \sigma_{appl}/R_{eL}$, the plate width W and the value of J_{crit} .

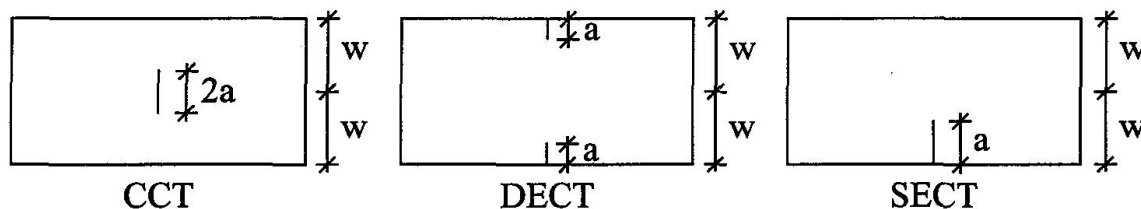


Fig. 12 Basic plate models and crack configurations for fracture mechanic assessment CCT: plate with centre crack -, DECT: plate with double edge crack, SECT: plate with single edge crack in tension

The basis of the determination of a_{crit} is the safety check where J_{appl} may be calculated for $\sigma_{appl} \leq \sigma_{gy}$ where σ_{gy} is the applied stress to achieve general yield in the net section. σ_{appl} is the applied stress for the relevant load combination. The values σ_{gy} may be taken as follows [17], [18]:

- plate with centre crack or single edge crack:

$$\sigma_{gy} = R_{eL} \cdot (1 - a/W) \quad (4)$$

- plate with double edge crack

$$\sigma_{gy} = R_{eL} \cdot (1 - a/W) \cdot (1 + 0.25 \cdot a/W). \quad (5)$$

The value for J_{appl} may be determined from:

$$J_{appl} = J_{gy} \cdot \left[1 - \left(1 - \left(\frac{\sigma_{appl}}{\sigma_{gy}} \right)^2 \right)^d \right] \quad (6)$$

where

$$J_{gy} = \frac{2 W \cdot R_{eL}^2 \cdot k_1 \cdot a / W \cdot (1 - a / W^{k_2}) \cdot k_3}{210000 \cdot (a / W + k_4)} \quad (7)$$

is the J-value for general yield in the net section and k_1, k_2, k_3, k_4 are fitting variables.

The accuracy of the approach from equations 6 and 7 may be taken from a comparison with FEM calculations as shown in Figure 13 for a plate with a centre crack.

An example for a graph that gives a_{crit} -values in dependency of $d = \sigma_{appl}/R_{eL}$ for various J-values for a plate with a centre crack is given in Figure 14.

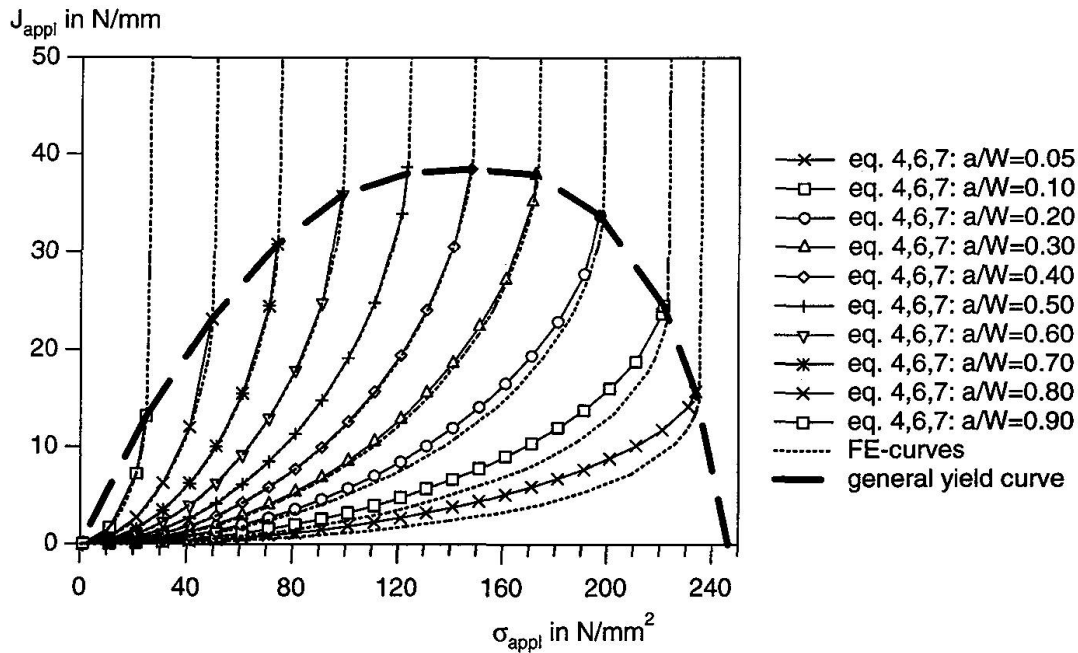
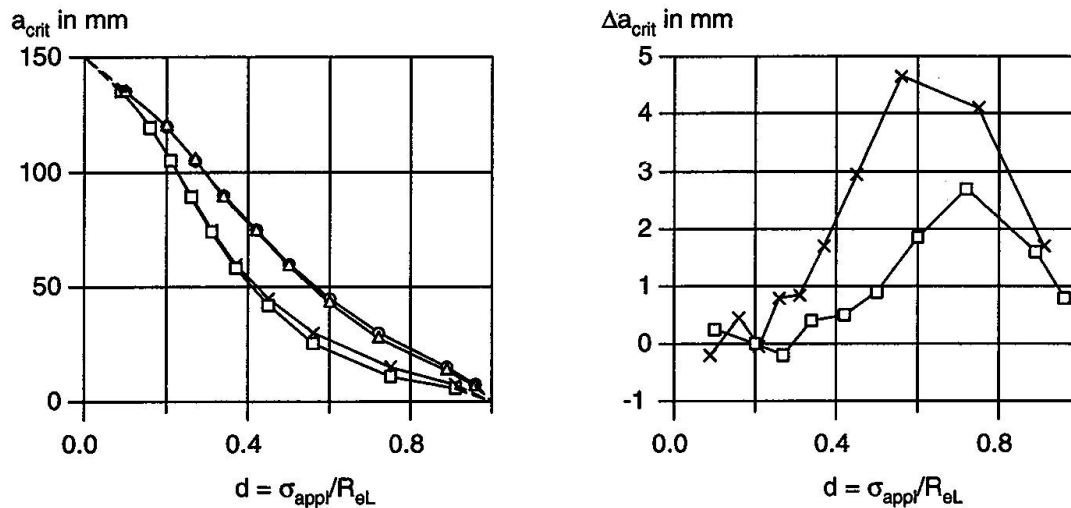


Fig. 13 Comparison of $\sigma_{appl} - J_{appl}$ curves from FEM and results with Equations (4), (6) and (7), plate with centre crack, $2W=300$ mm, $d=0.63$, $k_1=0.64$, $k_2=k_3=1.0$, $k_4=0.125$



a_{crit} - FE : \times : $J = 10$ N/mm ; \circ : $J = 20$ N/mm

a_{crit} - calc : \square : $J = 10$ N/mm ; \triangle : $J = 20$ N/mm

Δa_{crit} : $J = 10$ N/mm \times : $a_{FE} - a_{calc}$

Δa_{crit} : $J = 20$ N/mm \square : $a_{FE} - a_{calc}$

Fig. 14 Comparison of critical crack sizes ; FE-Analysis to Equations (4), (6) and (7), CCT, $2W=300$ mm

3.3 Model uncertainty

The model uncertainty for the determination of failure loads F_{Rk} was checked in [17] by comparison with 82 wide plate tests with the method given in Eurocode 3, Part 1.1 - Annex Z [6]. The check was carried out both with measured material strength and fracture toughness data for modern steels and wrought iron and with 5% fractile data for wrought iron as given in Table 1.

The failure load from equation 6 reads

$$F_{Rk,model} = \frac{\sigma_{gy} \cdot t \cdot B}{1000} \cdot \left(1 - \left(1 - \frac{J_{crit}}{J_{gy}} \right)^{1/d} \right)^{0.5} \quad [\text{kN}] \quad (8)$$

where $J_{crit} \leq J_{gy}$

From these statistical evaluations the safety factors γ_M^* for the prediction model were determined as $\gamma_M^* = 1,14 - 1,23$ when using measured material data and $\gamma_M^* = 1,07 - 1,09$ when using 5% fractile data of the material toughness J_{crit} and strength R_{eL} for wrought iron as given in table 1. Considering that the material toughness values are all determined for plane strain conditions instead of plane stress conditions which are the relevant toughness values for the structural behaviour of tension members with through thickness cracks up to plate thickness $t = 100$ mm [20] the following γ -Factors are proposed for Equation 7:

1. in case of using measured strength and toughness data

$$F_{Rd} = 1/\gamma_M^* \cdot F_{Rk} \text{ with } \gamma_M^* = 1,10$$

2. in case of using 5% fractile values for the material strength and toughness for wrought iron from Table 1

$$F_{Rd} = 1/\gamma_M^* \cdot F_{Rk} \text{ with } \gamma_M^* = 1,00.$$

References

1. HENSEN W. Grundlagen für die Beurteilung der Weiterverwendung alter Stahlbrücken. Dissertation, RWTH Aachen 1992
2. DAHL W., SCHUMANN O., SEDLACEK G. Method to Back Decision on Residual Safety of Bridges. IABSE Workshop Remaining Fatigue life of Steel Structures Lausanne 1990, IABSE Report Vol 59, 1990, S. 313-326.
3. SEDLACEK G., HENSEN W., BILD J., DAHL W., LANGENBERG P. Verfahren zur Ermittlung der Sicherheit von alten Stahlbrücken unter Verwendung neuester Erkenntnisse der Werkstofftechnik. Bauingenieur, 1992.
4. SEDLACEK G., HENSEN W. Nouvelles Methodes de calcul pour la rehabilitation des Ponts metalliques anciens. Construction Metallique, No 3, 1992.
5. SEDLACEK G., HENSEN W. New assessment methods for the residual safety of old steel bridges. Steel Research 64, No 8/9, 1993.
6. DAHL W., SEDLACEK G. Untersuchungen zur Ermittlung der Sicherheit und Restnutzungsdauer der Karl-Lehr-Brücke in Duisburg. Expertise for the town Duisburg, 1986.
7. DAHL W., SEDLACEK G. Untersuchungen zur Ermittlung der Sicherheit und Restnutzungsdauer der Anhalter-Bahn-Brücke in Berlin. Expertise for the railway authority in Berlin, 1989.
8. DAHL W., SEDLACEK G. Untersuchungen zur Ermittlung der Sicherheit und Restnutzungsdauer der U-Bahnbrücken zwischen Gleisdreieck und Bahnhof Möckernbrücke in Berlin. Expertise for the railway authority in Berlin, 1990.
9. DAHL W., LANGENBERG P., SEDLACEK G., STÖTZEL G. Sicherheitsüberprüfung von Stahlbrücken. DFG- Forschungsvorhaben Da85/62 und Se351/9.
10. EUROCODE 3, PART 1.1 Design of steel structures: General rules and rules for buildings - ANNEX Determination of design resistance from tests. Document CEN/ TC 250/SC 3/ N361E, Sept. 1993.
11. BRÜHWILER E. Essais de Fatigue sur des Poutres a Tripplis Double en per Puddle. Publication ICOM 159/1986.
12. BILD J. Beitrag zur Anwendung der Bruchmechanik bei der Lösung von Sicherheitsproblemen im Stahlbau. Dissertation, RWTH Aachen, 1988.
13. CHEREPANOW G.P. PMM 31 (1967) No. 3, p. 476/88.
14. RICE J.R., TRANCEY D.M. J. Mech. Phys. Solids 17 (1969), p. 201/17.
15. LANGENBERG P., DAHL W., HAN S. Bruchverhalten alter Stähle in genieteten Brücken - Bruchmechanische Sicherheitsanalyse und Bauteilversuche. DVM Tagung des AK Bruchvorgänge, 2/1996.
16. LANGENBERG P. Bruchmechanische Sicherheitsanalyse anrißgefährdeter Bauteile im Stahlbau. Dissertation, RWTH Aachen 1995.
17. STÖTZEL G. Verfahren zur zuverlässigen Bestimmung der Sicherheit bei Weiterverwendung alter Stahlbrücken. Dissertation in Vorbereitung, RWTH Aachen.
18. EHRHARDT H. Untersuchung zum Einfluß unterschiedlicher Fehlergeometrien auf das Versagensverhalten von Stahl auf der Grundlage von Großzugversuchen. Dissertation, RWTH Aachen 1988.
19. PARIS P., ERDOGAN F. A critical analysis of crack propagation laws. Journal of Basic Engineering , Trans ASME Series D, Vol. 85, pp. 528-534 (1963).

Leere Seite
Blank page
Page vide